OXFORD

Human Molecular Genetics, 2022, Vol. 31, No. 2 189–206

https://doi.org/10.1093/hmg/ddab230
Advance Access Publication Date: 14 August 2021
General Article

GENERAL ARTICLE

Myeloid cell-mediated targeting of LIF to dystrophic muscle causes transient increases in muscle fiber lesions by disrupting the recruitment and dispersion of macrophages in muscle

Ivan Flores[1], Steven S. Welc[2,3], Michelle Wehling-Henricks[4] and James G. Tidball[1,4,5,*]

[1]Molecular, Cellular & Integrative Physiology Program, University of California, Los Angeles, CA 90095-1606, USA, [2]Department of Anatomy, Cell Biology & Physiology, Indiana University School of Medicine, Indianapolis, IN 46202, USA, [3]Indiana Center for Musculoskeletal Health, Indiana University School of Medicine, Indianapolis, IN 46202, USA, [4]Department of Integrative Biology and Physiology, University of California, Los Angeles, CA 90095-1606, USA and [5]Department of Pathology and Laboratory Medicine, David Geffen School of Medicine at UCLA, University of California, Los Angeles, CA 90095, USA

*To whom correspondence should be addressed at: James G. Tidball, Molecular, Cellular & Integrative Physiology Program, University of California, Los Angeles, CA 90095-1606, USA. Tel: 310-206-3395; Fax: 310-825-8489; Email: jtidball@physci.ucla.edu

Abstract

Leukemia inhibitory factor (LIF) can influence development by increasing cell proliferation and inhibiting differentiation. Because of its potency for expanding stem cell populations, delivery of exogenous LIF to diseased tissue could have therapeutic value. However, systemic elevations of LIF can have negative, off-target effects. We tested whether inflammatory cells expressing a LIF transgene under control of a leukocyte-specific, CD11b promoter provide a strategy to target LIF to sites of damage in the *mdx* mouse model of Duchenne muscular dystrophy, leading to increased numbers of muscle stem cells and improved muscle regeneration. However, transgene expression in inflammatory cells did not increase muscle growth or increase numbers of stem cells required for regeneration. Instead, transgene expression disrupted the normal dispersion of macrophages in dystrophic muscles, leading to transient increases in muscle damage in foci where macrophages were highly concentrated during early stages of pathology. The defect in inflammatory cell dispersion reflected impaired chemotaxis of macrophages to C-C motif chemokine ligand-2 and local increases of LIF production that produced large aggregations of cytolytic macrophages. Transgene expression also induced a shift in macrophage phenotype away from a CD206+, M2-biased phenotype that supports regeneration. However, at later stages of the disease when macrophage numbers declined, they dispersed in the muscle, leading to reductions in muscle fiber damage, compared to non-transgenic *mdx* mice. Together, the findings show that macrophage-mediated delivery of transgenic LIF exerts differential effects on macrophage dispersion and muscle damage depending on the stage of dystrophic pathology.

Received: May 10, 2021. **Revised:** August 4, 2021. **Accepted:** August 5, 2021

Introduction

A recently developed strategy for targeting therapeutic molecules to dystrophic muscle exploits inflammatory cells as natural vectors to selectively express and deliver potentially beneficial proteins to diseased muscle (1). Because inflammatory cells rapidly invade dystrophic muscle specifically at the times and locations where pathology is active, and afterwards they naturally reduce in numbers and activity when pathology attenuates, they provide a rapidly responsive, intrinsic system to target disease. This targeting approach is especially valuable in diseases such as Duchenne muscular dystrophy (DMD) which is unpredictably 'asynchronous' (2), in which different muscles and even different groups of muscle fibers in the same muscle occur at different stages of injury and repair. As a consequence, foci of muscle damage and necrosis can exist hundreds of micrometers from sites where muscle fibers are experiencing regeneration or hundreds of micrometers from sites where muscle fibers have not experienced damage.

Leukemia inhibitory factor (LIF) has long been expected to have potential therapeutic benefits in treating muscular dystrophy, attributable to its numerous influences on myogenesis. For example, LIF stimulates myoblast proliferation *in vitro* (3–5), which is mediated through the Jak2-Stat3 pathway (6) and may also expand their numbers *in vitro* by reducing their frequency of apoptosis (7). In addition, LIF can inhibit the formation of post-mitotic, multinucleated myotubes *in vitro* by inhibiting myoblast differentiation, which may also lead to expansion of myoblast numbers (7). LIF can also affect growth of myotubes at later stages of myogenesis *in vitro* by increasing their protein synthesis via an Akt-mediated mechanism (8). These pro-myogenic, anabolic influences of LIF on muscle cells *in vitro* are reflected in the responses of muscle to changes in LIF expression or delivery following muscle injury or in muscle disease. Elevations of systemic LIF levels in mice experiencing acute muscle injury or denervation cause faster growth of regenerative muscles (9,10) and muscle regeneration following acute injury is slower in LIF-null mutant mice (11). Similarly, increased delivery of LIF to diaphragm muscles in the *mdx* mouse model of DMD produced larger muscle fibers (12).

Although those *in vitro* and *in vivo* effects of LIF on myogenesis support its potentially beneficial role in the treatment of injured and diseased muscle, increased delivery of LIF can also cause negative, off-target effects. For example, prolonged, systemic elevations of LIF in cancer can significantly increase wasting of non-diseased muscle fibers (13–15), emphasizing the importance of targeting LIF specifically to sites of active muscle pathology, to enhance myogenesis at those sites. We previously addressed this obstacle to targeting LIF specifically to sites of pathological muscle damage by transplanting transgenic bone marrow cells (BMCs) that expressed a LIF transgene under control of the leukocyte-specific, CD11b promoter (CD11b/LIF transgene) (1). Because the transplanted cells subsequently differentiated into inflammatory cells in which the LIF transgene was expressed at high levels at sites of muscle damage, the system provided a targeted delivery of LIF to sites of pathology. The primary beneficial outcome of that therapeutic intervention was a reduction in fibrosis, which is a debilitating feature of muscular dystrophy (1).

Expression of the CD11b/LIF transgene in *mdx* mice also produced a significant increase in the number of regenerating fibers in dystrophic muscle, which could represent either a beneficial or a detrimental effect of targeted delivery of LIF. On one hand, the outcome could reflect improved muscle regeneration, which would be consistent with many of the influences of LIF on muscle cells *in vitro*. Alternatively, the increase in muscle regeneration could also result from amplification of muscle fiber damage, which would lead to more repair. In either scenario, the LIF-induced changes in the extent of regeneration of dystrophic muscle could be caused by perturbations of the immune response to muscular dystrophy, because LIF can modulate the inflammatory response to injury or disease (16,17) and perturbations of the immune response to muscular dystrophy can either worsen muscle damage (18–21) or improve repair (1,21–26).

In the present investigation, we test whether expression of the CD11b/LIF transgene in inflammatory cells leads to changes in the function of inflammatory cells that can influence injury or growth of dystrophic muscles. In particular, we assess whether the CD11b/LIF transgene influences the numbers, distribution or phenotype of innate immune cells or specific macrophage subpopulations in dystrophic, *mdx* muscle and whether their cytotoxicity or chemotactic response is affected. We also test whether expression of the transgene amplifies muscle fiber damage *in vivo* or influences the regeneration or growth of dystrophic muscles over the course of *mdx* dystrophy. Together, the findings will contribute to the assessment of whether targeted delivery of the CD11b/LIF transgene to dystrophic muscle has promising therapeutic potential.

Results

We confirmed that LIF expression was elevated in macrophages located in muscles of LIF/*mdx* mice by isolating macrophages from pooled limb muscles obtained from LIF/*mdx* and WT/*mdx* mice and assaying for LIF expression by QPCR (Fig. 1A). We next investigated whether LIF protein occurred at elevated levels where macrophages accumulated in transgenic muscles. Labeling of adjacent muscle cross-sections for CD68+ macrophages (Fig. 1B), LIF protein (Fig. 1C) and CD206+ macrophages (Fig. 1D) showed that LIF protein content was increased at sites enriched with CD68+ macrophages but with fewer CD206+ macrophages. Our previous findings demonstrated that LIF protein content was greater in inflammatory lesions of LIF/*mdx* muscles compared to WT/*mdx* muscles (1). We also assayed whether there were higher levels of LIF protein in muscle fibers of LIF/*mdx* mice compared to fibers in WT/*mdx* mice, which would indicate ectopic expression of the gene in muscle, but found no significant difference between the two genotypes (Supplementary Material, Fig. S1). These data validate that the overexpression of LIF in whole muscles of LIF/*mdx* mice results from LIF expression by transgenic macrophages.

We then tested whether the greater co-localization of LIF with M1-biased macrophages was attributable to greater expression of LIF mRNA by M1-biased macrophages compared to M2-biased macrophages. First, we validated that unstimulated (Th0), bone marrow-derived macrophages (BMDMs) isolated from LIF/*mdx* mice (CD11b/LIF+ BMDMs) expressed significantly higher levels of LIF than BMDMs from WT/*mdx* mice (CD11b/LIF- BMDMs) (Fig. 1E). We then assayed whether expression levels of LIF were affected by whether CD11b/LIF+ BMDMs were stimulated with Th1 (TNFα and IFNγ) or Th2 cytokines (IL4 and IL10). Th1 cytokines are expressed during pro-inflammatory responses and activate macrophages toward an M1 phenotype (27–31). Th2 cytokines downregulate inflammation and activate an M2 phenotype in macrophages (20,21,23,27,29,30,32–35). Our results show that stimulation of CD11b/LIF+ BMDMs with Th1 cytokines approximately doubled their production of LIF (Fig. 1E). However, stimulation of CD11b/LIF+ BMDMs with Th2 cytokines

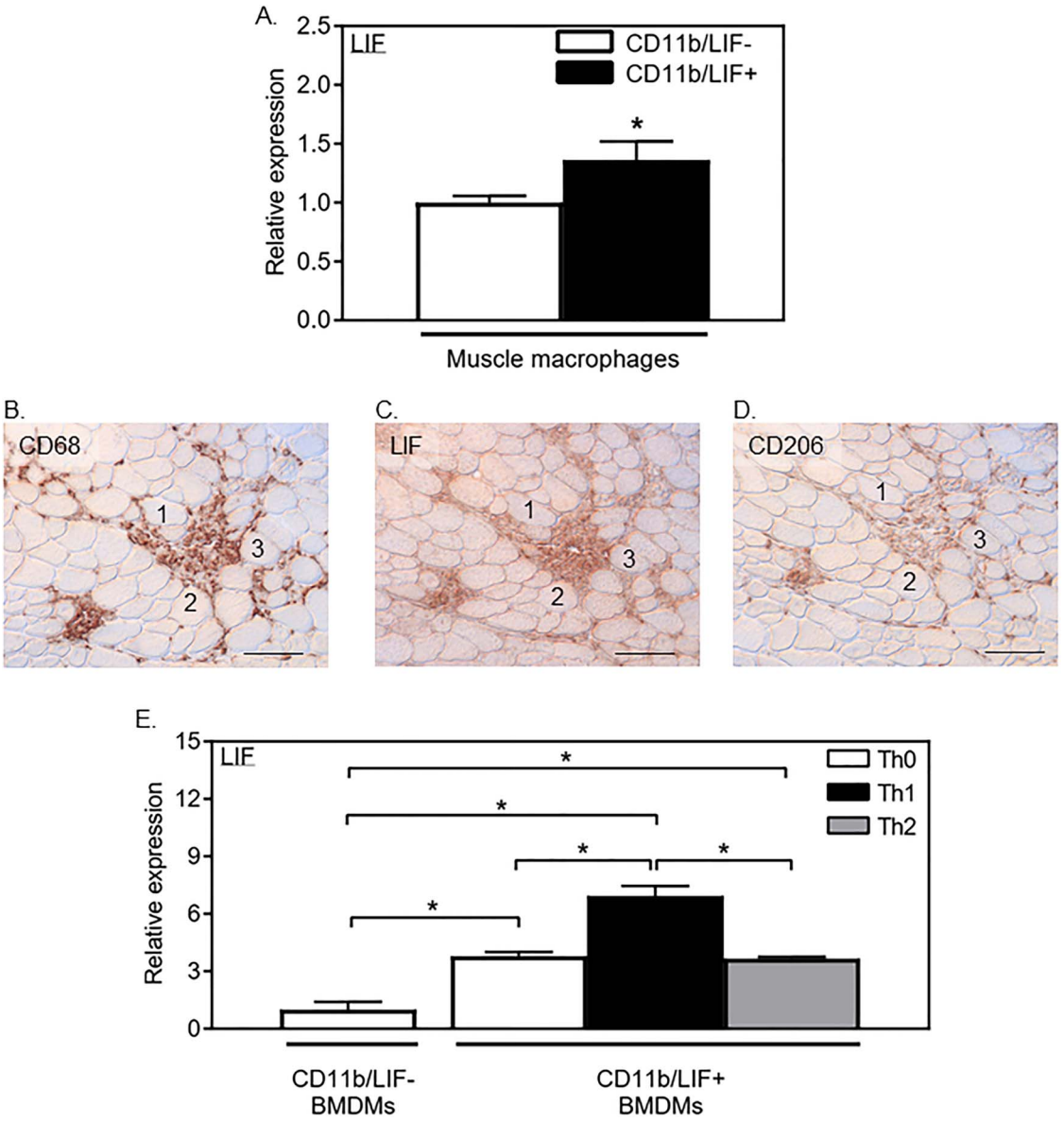

Figure 1. LIF expression is elevated in intramuscular macrophages of LIF/*mdx* mice. Histogram of LIF expression in macrophages isolated from the hind limb muscles of WT/*mdx* and LIF/*mdx* mice. **(A)**. * indicates significant difference compared to CD11b/LIF- muscle macrophages ($P < 0.05$). *P*-values are based on a two-tailed t-test. $N = 5$ for WT/*mdx* and $n = 3$ for LIF/*mdx* mice. Bars = SEM. Immunolabeling of adjacent cross-sections with anti-CD68 **(B)**, anti-LIF **(C)** and anti-CD206 **(D)** shows local, elevated LIF protein content at sites that are most highly enriched with CD68+ macrophages in LIF/*mdx* muscles. Fibers that are numbered '1,' '2' or '3' are individual fibers that appear in adjacent sections, to provide reference points in the sections. Scale bars = 50 μm. QPCR analysis of CD11b/LIF- and CD11b/LIF+ BMDMs that were unstimulated (Th0) or stimulated with Th1 or Th2 cytokines show increased expression of *lif* in M1-biased BMDMs **(E)**. * indicates significant difference between the two groups indicated by the ends of the horizontal brackets ($P < 0.05$). N = 3 for all groups. *P*-values are based on two-way ANOVA with Tukey's multiple comparisons test. Bars = SEM.

did not affect LIF expression relative to Th0 transgenic BMDMs (Fig. 1E). These findings show that expression of LIF in LIF/*mdx* mice is highest in M1-biased macrophages, which indicates that LIF is delivered to muscles in LIF/*mdx* mice primarily by pro-inflammatory macrophages.

CD11b/LIF transgene expression reduces CD206+ macrophage numbers

We assessed the effects of CD11b/LIF transgene expression on muscle inflammation in *mdx* mice during the acute onset of pathology (1-month-old), successful regeneration (3-months-old) and during the period of progressive degeneration (12-months-old) that includes progressive reductions of satellite cell numbers and function, progressive reductions in muscle fiber size, progressive increases in fibrosis and progressive reductions in muscle strength (36–38). Although the total number of CD11b + innate immune cells in *mdx* muscle declined following the acute peak of pathology (Fig. 2 A-F; M), transgene expression did not affect CD11b + cell numbers at any stage (Fig. 2M). This negative result resembles the absence of treatment effect of CD11b/LIF transgene expression on CD68+ macrophages in *mdx* muscle (1). However, when we assayed whether the transgene affected the numbers of CD206+,

M2-biased macrophages (Fig. 2G-L, N), we observed a transgene-mediated reduction in the numbers of CD206+ macrophages at 1-month and 3-months of age, although their numbers returned to non-transgenic *mdx* levels by 12-months of age (Fig. 2N). These findings indicate that CD11b/LIF transgene expression selectively reduces the numbers of CD206+ macrophages in dystrophic muscles at early stages of the disease.

Macrophage-mediated delivery of transgenic LIF reduces macrophage dispersion

Although we found no effect of the CD11b/LIF transgene on total numbers of CD11b + innate immune cells in *mdx* muscle, the transgene dramatically influenced the dispersion of immune cells in muscle. At the 1-month time-point, CD11b + (Fig. 3A), CD68+ (Fig. 3B) and CD206+ (Fig. 3C) macrophages were broadly dispersed throughout the muscles of WT/*mdx* mice. In contrast, CD11b + (Fig. 3D) and CD68+ (Fig. 3E) showed clumped population dispersions in LIF/*mdx* muscles, despite no effect of the transgene on the total numbers in muscle of either cell population (Fig. 2M) (1). CD206+ macrophages also exhibited a clumped population dispersion in inflammatory lesions of LIF/*mdx* mice (Fig. 3F), although the effect was not as apparent as it was for CD68+ macrophages. The transgene did not affect macrophage dispersion at the 3-month (Fig. 3G-L) or 12-month (data not shown) time-points.

CD11b/LIF+ macrophages have reduced chemotactic potential

The reduced numbers and dispersion of macrophages in LIF/*mdx* muscles suggest that elevated levels of LIF can affect macrophage chemotaxis within dystrophic muscles. We assayed whether LIF could affect C-C motif chemokine ligand-2 (CCL2) production in BMDMs because CCL2 is a potent chemoattractant that plays a dominant role in recruiting macrophages to injured tissues, including muscle (39–49). Analysis of the proportion of F4/80+ macrophages that express CCL2 (F4/80 + CCL2+ cells) showed that macrophages are an *in vivo* source of CCL2 in LIF/*mdx* muscles (Fig. 4A–D). We observed a reduction of more than 20% in the proportion of macrophages expressing CCL2 in muscles of 1-month-old LIF/*mdx* mice and observed a strong trend for the same effect at the 3-month time-point (Fig. 4E). We confirmed that the reduction in CCL2 expression was attributable to direct effects of LIF on macrophages by stimulating BMDMs generated from wild-type C57 mice (WT BMDMs) with recombinant LIF (rLIF), which reduced CCL2 secretion into the medium, relative to vehicle-stimulated BMDMs (Fig. 4F). Similarly, BMDMs generated from LIF/mdx mice (CD11b/LIF+ BMDMs) secreted less CCL2 than BMDMs generated from WT/*mdx* mice (CD11b/LIF- BMDMs) in the absence of rLIF stimulation (Fig. 4G). QPCR analysis confirmed decreased expression of *ccl2* by CD11b/LIF+ BMDMs (Fig. 4H).

In addition to reducing available CCL2, transgene expression may also reduce the chemotactic response of macrophages to CCL2. We used a chemotaxis assay to test whether CD11b/LIF transgene expression could reduce the migration of BMDMs in response to CCL2 and found that Th0 and M2-biased, CD11b/LIF- BMDMs were responsive to CCL2 (Fig. 4I). However, expression of the transgene by BMDMs eliminated their chemotactic response to CCL2 (Fig. 4I). Collectively, our results show that elevated expression of LIF by transgenic macrophages reduces their expression of CCL2 and their chemotactic response to CCL2, which may contribute to the disruption of normal dispersion of macrophages in *mdx* muscles.

Muscle fiber damage is increased at sites of increased macrophage accumulation

Prolonged activation of M1-biased macrophages in *mdx* muscles can exacerbate fiber damage through muscle membrane lysis (22,50,51). We assayed whether the localized increase in CD68+ macrophages could affect fiber damage in LIF/*mdx* muscles. Labeling of injured (albumin+) fibers (52) in 1-month-old muscles of WT/*mdx* (Fig. 5A) and LIF/*mdx* (Fig. 5B) mice showed albumin+ fiber clusters that resembled CD68+ macrophage clusters at the same time-point (Fig. 3). Labeling of adjacent cross-sections of LIF/*mdx* muscles for CD68+ macrophages (Fig. 5C), albumin+ fibers (Fig. 5D) and CD206+ macrophages (Fig. 5E) confirmed co-localization of injured fibers to areas enriched with CD68+ macrophages and relatively few CD206+ macrophages. Quantification of albumin+ fibers at each stage of the pathology showed a transient increase in fiber damage of LIF/*mdx* muscles at 1- and 3-months of age (Fig. 5F). However, at 12-months of age when macrophages are broadly dispersed in muscles, LIF/*mdx* muscles showed significantly less fiber damage (Fig. 5F). We also assayed whether transgene expression affected variance of muscle fiber cross-sectional area, which is also an indicator of muscle pathology (53,54), and found a transient increase in fiber area variance at the 1-month time-point (Fig. 5G). Increased variance occurs when there is increased damage because there are more injured fibers and each injured fiber can be at a different stage of repair and growth, which increases size variance in the population.

In addition to increasing muscle damage by increasing the numbers of M1-biased macrophages at sites of injury, the transgene may also increase the cytotoxic potential of individual macrophages. To test this possibility, we performed a fluorescence microscopy-based cytotoxicity assay to measure macrophage-mediated lysis of myoblasts. In this approach, non-labeled BMDMs were co-cultured with muscle cells that were pre-labeled with the fluorescent marker, CFSE (488 nm emission). Following the cytotoxicity period, lysed cells were labeled using GelRed (594 nm emission), a cell membrane-impermeable DNA-binding dye. The proportion of lysed muscle cells (CFSE+GelRed+ cells) out of total muscle cells (CFSE+ cells) was quantified using fluorescence microscopy (Fig. 6A–F). We validated the sensitivity of this assay by showing a positive correlation between numbers of lysed muscle cells and numbers of wild-type BMDMs present in the co-cultures (Fig. 6G). We used this approach to test the cytotoxic potential of CD11b/LIF- and CD11b/LIF+ BMDMs. The BMDMs were polarized to a cytolytic phenotype using Th1 cytokines or left in an unpolarized state prior to co-culturing the BMDMs with muscle cells. Although Th1-stimulated BMDMs of both genotypes showed increased cytotoxicity compared to genotype-matched, unpolarized BMDMs, transgene expression had no effect on the cytotoxic potential of Th1-stimulated or unstimulated BMDMs (Fig. 6H). Our results indicate that increased muscle damage observed in LIF/*mdx* mice is caused by increased, localized accumulation of M1-biased macrophages at inflammatory lesions and not by increased cytotoxic potential of CD11b/LIF+ macrophages.

LIF transgenic macrophages accumulate at sites of *mdx* muscle growth and repair

Our previous work showed an increase in the numbers of regenerating, developmental myosin heavy chain-positive (dMHC+) fibers in LIF/*mdx* muscles (1), which suggested the possibility that those sites of repair could be associated with elevated numbers of transgenic macrophages. We tested

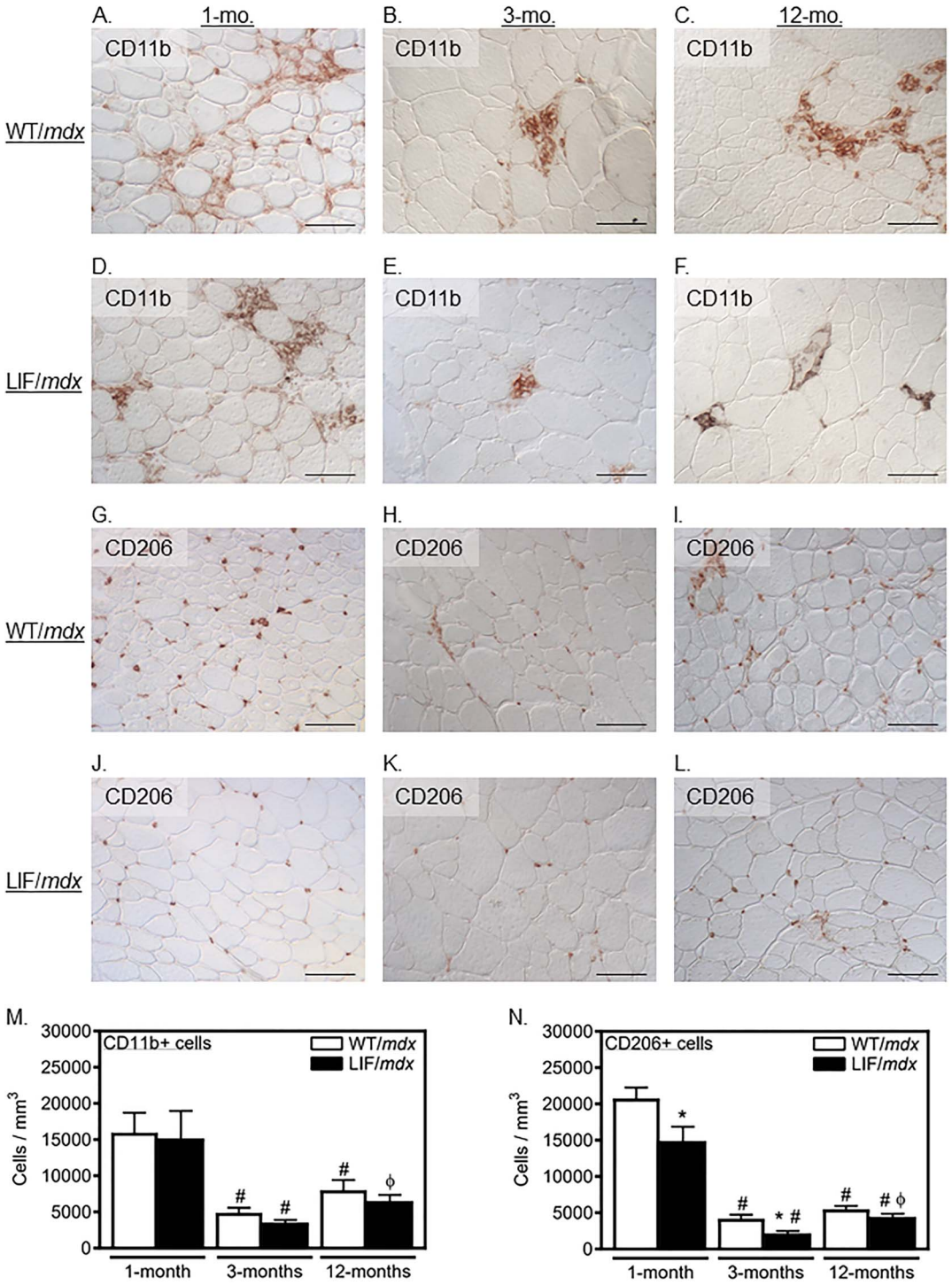

Figure 2. CD11b/LIF transgene expression does not affect total numbers of leukocytes in dystrophic muscle, but specifically reduces numbers of CD206+ macrophages. Cross-sections of WT/*mdx* **(A-C, G-I)** and LIF/*mdx* **(D-F, J-L)** muscles were immunolabeled with anti-CD11b **(A–F)** and anti-CD206 **(G–L)** to identify innate immune cells and M2-biased macrophages, respectively. Muscle sections were labeled at the 1- **(A, D G, J)**, 3- **(B, E, H, K)** and 12-month **(C, F, I, L)** time-points. Scale bars = 50 μm. Numbers of CD11b + **(M)** and CD206+ **(N)** cells were normalized to muscle volume in mice of both genotypes along the course of pathology and show a reduction of CD206+ macrophages in LIF/*mdx* muscles. * indicates significant difference compared to age-matched, WT/*mdx* mice ($P < 0.05$). # and Φ indicate significant difference compared to 1- and 3-month mice of the same genotype, respectively. *P*-values are based on two-tailed t-tests. CD11b + cell data: $n = 5$ for all groups. CD206+ cell data: $n = 7$ for both groups at the 1-month time-point and $n = 5$ for all groups at the 3- and 12-month time-points. Bars = SEM.

whether high densities of macrophages were associated with elevated numbers of dMHC+ fibers by labeling adjacent muscle sections for CD68+ macrophages (Fig. 7A, D), dMHC+ fibers (Fig. 7B, E) and CD206+ macrophages (Fig. 7C, F), which showed that regions of muscle regeneration were most-enriched with CD68+ macrophages. We then assayed whether the proportion

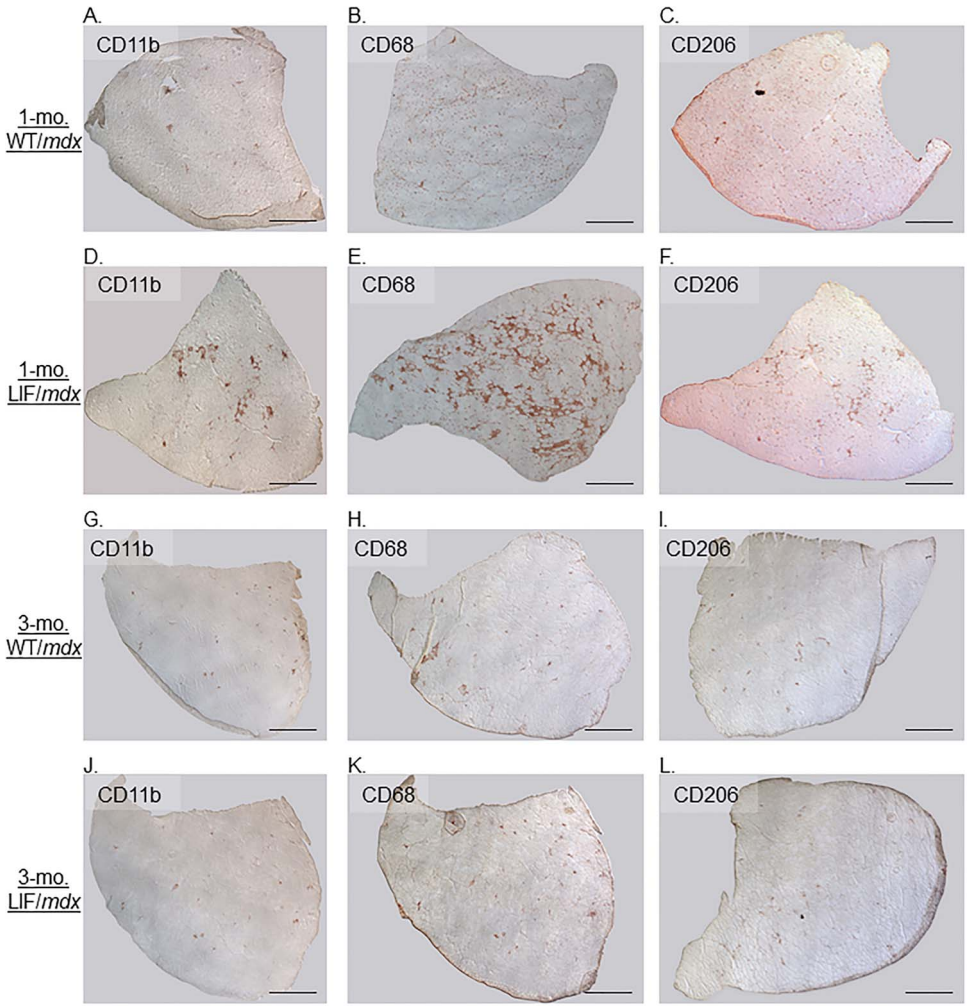

Figure 3. The LIF/transgene inhibits dispersal of macrophages in dystrophic muscles. Muscle cross-sections of 1- **(A–F)** and 3-month-old **(G–L)** TA muscles from WT/*mdx* **(A-C, G–I)** and LIF/*mdx* **(D–F, J–L)** mice were immunolabeled for macrophage markers to assess immune cell localization. Labeling with anti-CD11b **(A, D, G, J)**, anti-CD68 **(B, E, H, K)** and anti-CD206 **(C, F, I, L)** shows that transgene expression modifies macrophage dispersion in LIF/*mdx* mice at 1-month, but not at 3-months of age. Scale bars = 500 μm.

of CD68+ macrophages that were located at sites of muscle regeneration was greater in LIF/*mdx* muscles and observed a nearly 2-fold increase in the density of CD68+ cells at areas of regeneration in LIF/*mdx* muscles compared to WT/*mdx* muscles and found that CD68+ macrophages in LIF/*mdx* muscles were 3.7-fold more concentrated at regenerating areas than non-regenerating areas (Fig. 7G–K). Thus, CD11b/LIF transgene expression increased the density of CD68+ macrophages at sites of muscle regeneration.

CD11b/LIF expression does not affect *mdx* muscle growth or repair

The observation that LIF transgenic macrophages were present at high numbers at sites of dMHC+ fibers suggested two interpretations of the findings. First, the transgenic macrophages may promote muscle growth and regeneration or the elevated numbers of dMHC+ fibers may occur at sites where macrophages induced cytolysis, leading to subsequent repair. We tested whether transgenic macrophages promoted growth of *mdx* muscles by assaying for treatment effects on muscle mass or muscle fiber size. However, LIF/*mdx* mice showed no significant differences in muscle mass (Fig. 8A, B), fiber size (Fig. 8C–F) or number of fibers per muscle (Fig. 8G) at the 1-, 3- and 12-month time-points. In addition, expression of the transgene did not affect the numbers of Pax7+, MyoD+ or myogenin+ cells in *mdx* muscle (Fig. 9A–D). Our results indicate that macrophage-mediated delivery of transgenic LIF does not have a significant effect on muscle growth or regeneration during the course of *mdx* dystrophy.

Discussion

The primary finding in our investigation is that expression of a CD11b/LIF transgene by inflammatory cells in dystrophic muscle amplifies muscle fiber damage during the early peak of *mdx* muscle pathology. However, as inflammatory cell numbers diminished and their dispersal increased during progressive stages of the pathology, the detrimental effect of the transgene declined. By 12 months of age, expression of the transgene produced a significant reduction of fiber damage. The amplification of fiber damage early in the disease is attributable to high, local concentrations of CD68+ macrophages, which can lyse *mdx* muscle fibers through a free-radical-mediated mechanism (22,51).

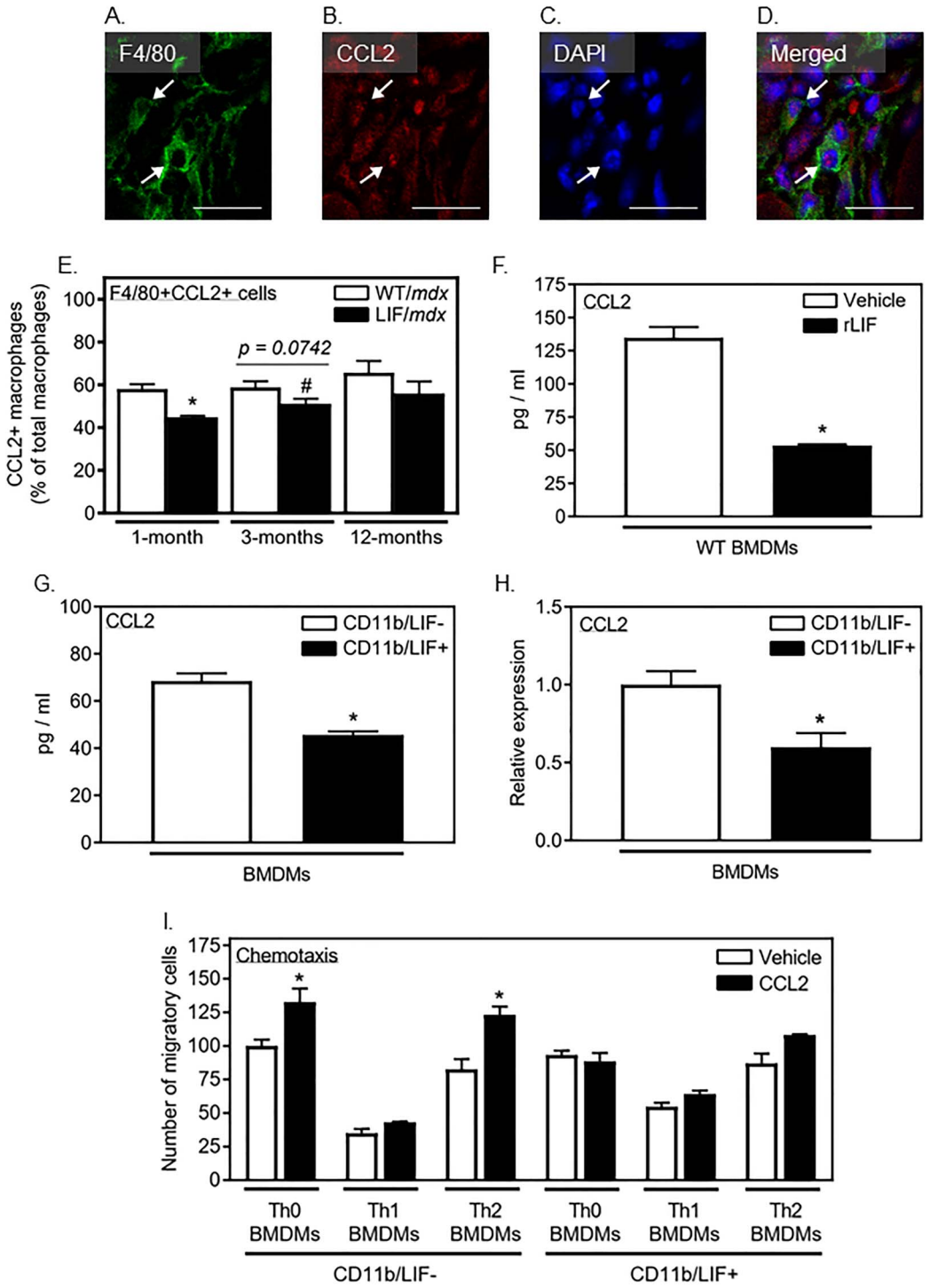

Figure 4. The CD11b/LIF transgene reduces CCL2 expression in CD11b/LIF+ macrophages and reduces chemotaxis to CCL2. Cross-sections labeled with anti-F4/80 **(A)** and anti-CCL2 **(B)** show that macrophages are a source of CCL2 in *mdx* muscles **(A–D)**. The arrows point to F4/80 and CCL2 double-positive cells. Scale bars = 20 μm. The proportion of F4/80+ macrophages that express CCL2 (F4/80 + CCL2+) is reduced in the muscles of LIF/*mdx* mice **(E)**. * indicates significant difference compared to age-matched, WT/*mdx* mice ($P < 0.05$). # indicates significant difference compared to 1-month-old mice of the same genotype ($P < 0.05$). $N = 5$ for all groups except WT/*mdx* muscles at the 3-month time-point ($n = 4$). ELISA of conditioned media shows reduced secretion of CCL2 from WT BMDMs treated with rLIF **(F)**. * indicates significant difference compared to vehicle-treated BMDMs ($P < 0.05$). $N = 5$ for both groups. ELISA of conditioned media from CD11b/LIF- and CD11b/LIF+ BMDMs shows reduced secretion of CCL2 mediated by transgene expression **(G)**. * indicates significant difference compared to CD11b/LIF- BMDMs ($P < 0.05$). $N = 5$ for both groups. QPCR analysis of CD11b/LIF- and CD11b/LIF+ BMDMs confirms the reduced secretion of CCL2 shown in **(G)** is caused by reduced expression of *ccl2* in CD11b/LIF+ BMDMs **(H)**. * indicates significant difference compared to CD11b/LIF- BMDMs ($P < 0.05$). $N = 5$ for CD11b/LIF- BMDMs and $n = 4$ for CD11b/LIF+ BMDMs. *In vitro* analysis of the chemotactic response of Th0-, Th1- and Th2-stimulated BMDMs shows reduced response to CCL2 from CD11b/LIF+ BMDMs **(I)**. * indicates significant difference compared to genotype-matched BMDMs receiving the same stimulation ($P < 0.05$). $N = 3$ for all groups except CD11b/LIF+ BMDMs with a Th0 and Th2 activation ($n = 2$). *P*-values are based on two-tailed t-test for all data. Bars = SEM.

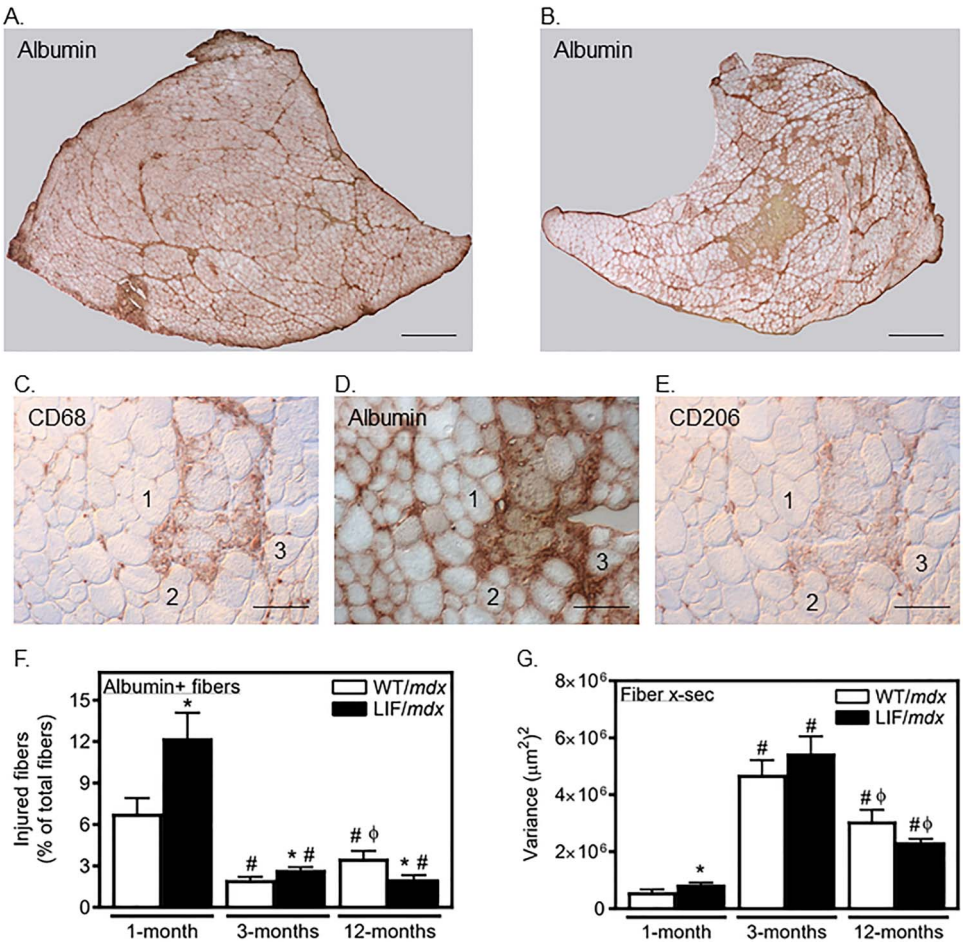

Figure 5. Muscle fiber damage is more extensive in LIF/*mdx* muscles at sites of macrophage accumulation. Cross-sections from 1-month-old WT/*mdx* **(A)** and LIF/*mdx* **(B)** muscles labeled with anti-albumin show injured fiber clusters that resemble CD68+ macrophage dispersion (Fig. 3B and 3E). Scale bars = 500 μm. Immunolabeling of adjacent cross-sections from LIF/*mdx* muscles with anti-CD68 **(C)**, anti-albumin **(D)** and anti-CD206 **(E)** shows greater co-localization of injured fibers with CD68+ macrophages relative to CD206+ macrophages. Fibers that are numbered '1,' '2' or '3' are individual fibers that appear in adjacent sections, to provide reference points in the sections. Scale bars = 50 μm. Transgene expression transiently increases the dystrophic pathology, as shown by an increase in the proportion of albumin+ fibers **(F)** and muscle fiber CSA variance **(G)** in LIF/*mdx* mice. * indicates significant difference compared to age-matched, WT/*mdx* mice ($P < 0.05$). # and Φ indicate significant difference compared to 1- and 3-month mice of the same genotype, respectively. *P*-values are based on two-tailed t-tests. Albumin+ fibers: $n = 5$ for all groups. Fiber variance: $n = 5$ for all groups except LIF/*mdx* samples at the 12-month time-point ($n = 4$). Bars = SEM.

Although the cytotoxicity of the transgenic macrophages did not differ from wild-type macrophages, the extent of muscle membrane lysis increased as numbers of macrophages increased *in vitro* or in inflammatory lesions *in vivo*; thus, the defect in CD68+ macrophage dispersal in the muscle produced high densities of cytolytic cells at foci of muscle fiber damage.

The high, local concentrations of muscle macrophages that were caused by the CD11b/LIF transgene occurred despite previous findings which showed that elevated LIF expression reduced total numbers of F4/80+ monocytes/macrophages that were recruited to *mdx* muscles at early stages of the pathology (1). This inhibitory effect on recruitment of monocytes/macrophages reflects some specificity of the influence of transgenic LIF on specific leukocyte populations because we found no effect of transgene expression on the numbers of CD11b + innate immune cells in *mdx* muscle. CD11b is expressed by monocytes and macrophages, but it is also expressed by basophils, neutrophils, eosinophils and NK cells, all of which are present in elevated numbers in *mdx* muscles (55–58). This tells us that elevated LIF expression does not reduce the aggregate numbers of innate immune cells in dystrophic muscle, but is more specifically inhibitory for monocytes/macrophages.

The selective reduction in monocytes/macrophage caused by elevated LIF is contrary to expectations based on other investigations. For example, *in vivo* observations have shown that the recruitment of macrophages to sites of tissue injury in the peripheral or central nervous system is reduced in LIF-null mutant mice (59) and *in vitro* findings have demonstrated that LIF is directly chemoattractive to macrophages and other myeloid cells (59,60). Our findings indicate that the reduction in macrophage recruitment caused by increased LIF is attributable to inhibition of powerful chemotactic signaling by CCL2 by elevated LIF expression. CCL2 plays a central role in regulating the traffic of immune cells to sites of muscle injury (61,62), intramuscular macrophages that express CCL2 play a major role in recruiting leukocytes to acutely injured muscles (63) and *mdx* muscle cells and inflammatory cells can release CCL2 to promote inflammation (64). Expression of the CD11b/LIF transgene reduced the production of CCL2 in macrophages and reduced the chemotactic response of macrophages to CCL2, both of which

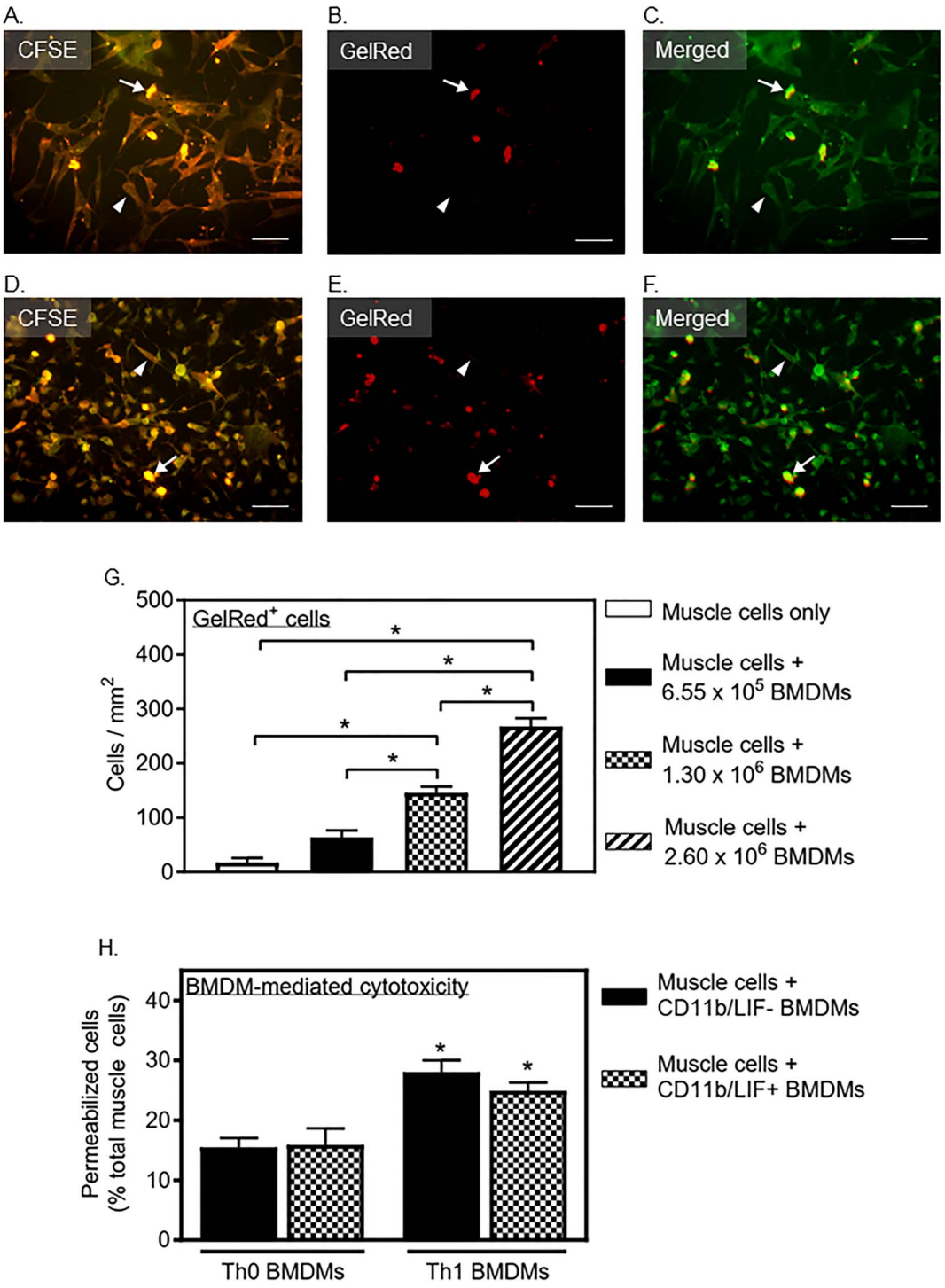

Figure 6. Expression of the CD11b/LIF transgene does not affect macrophage cytotoxic potential. Muscle cells were cultured in the absence **(A–C)** and presence of Th1-activated BMDMs **(D–F)**. Images of CFSE+ **(A, D)** and GelRed+ **(B, E)** muscle cells show an increase in the number of permeabilized muscle cells (CFSE+GelRed+; **C, F**) in the presence of Th1-activated BMDMs. The arrowheads indicate examples of non-permeabilized muscle cells (CFSE+GelRed-). The arrows indicate examples of permeabilized muscle cells (CFSE+GelRed+). Scale bars = 20 μm. Quantification of permeabilized cells shows an increase in muscle cell permeabilization with increasing numbers of Th1-stimulated BMDMs present in the co-cultures **(G)**. * indicates significant difference between the two groups indicated by the ends of the horizontal brackets ($P < 0.05$). *P*-values are based on one-way ANOVA with Tukey's multiple comparisons test. $N = 3$ for all groups except muscle cells only ($n = 2$). The proportion of permeabilized muscle cells is increased in co-cultures with Th1-stimulated BMDMs, but transgene expression does not affect BMDM-mediated permeabilization **(H)**. * indicates significant difference compared to genotype-matched, unstimulated BMDMs ($P < 0.05$). *P*-values are based on two-tailed t-tests. $N = 3$ for all groups. Bars = SEM for all data graphs.

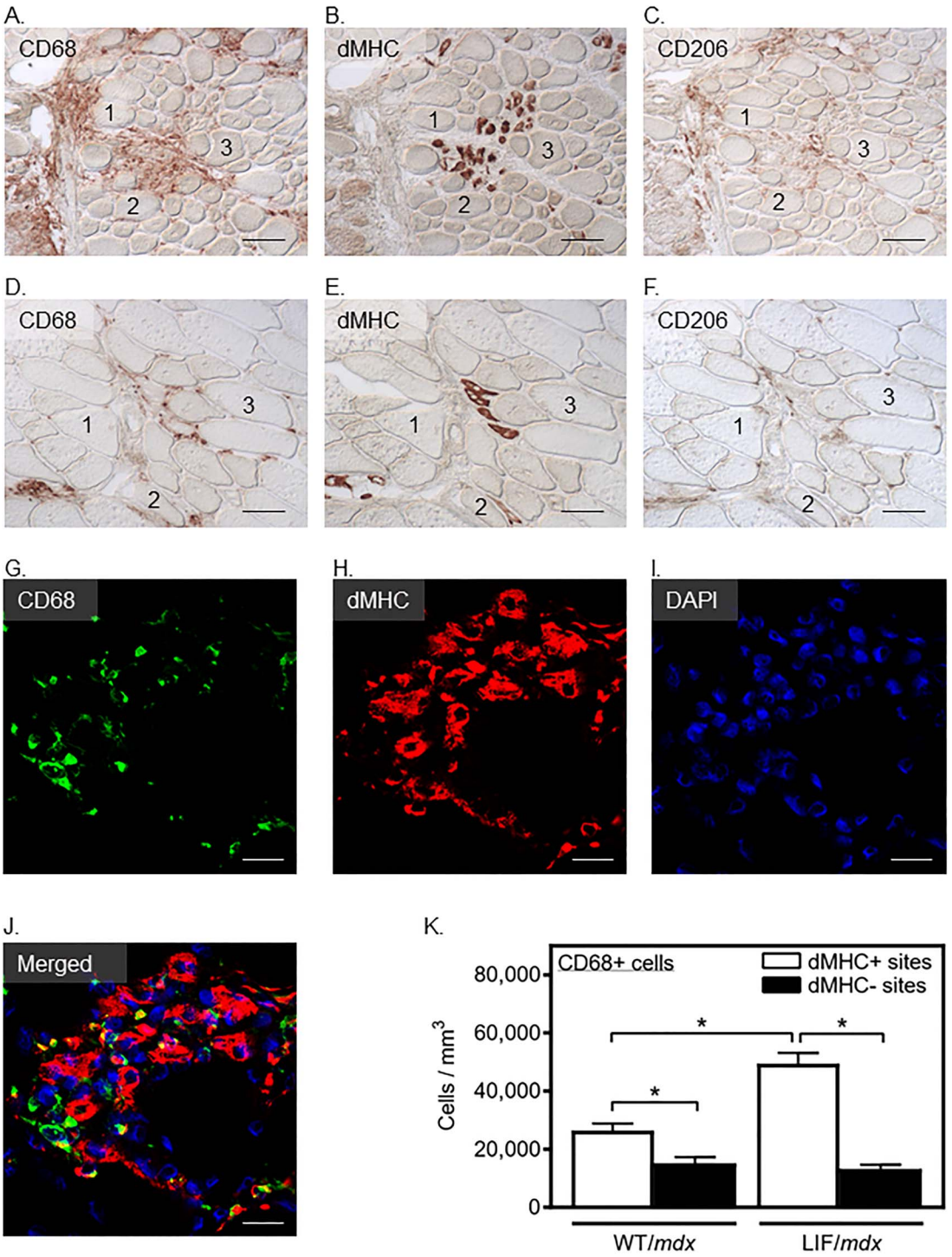

Figure 7. Macrophages accumulate at sites of muscle growth and repair in LIF/*mdx* muscles. Labeling of adjacent cross-sections from 1- **(A–C)** and 3-month **(D–F)** LIF/*mdx* muscles with anti-CD68 **(A, D)**, anti-dMHC **(B, E)** and anti-CD206 **(C, F)** show increased numbers of dMHC+ fibers in areas enriched with CD68+ macrophages. Fibers that are numbered '1,' '2' or '3' are individual fibers that appear in adjacent sections, to provide reference points in the sections. Scale bars = 50 μm. Cross-sections immunolabeled with anti-CD68 **(G)** and anti-dMHC **(H)** show clumped distributions of CD68+ macrophages at sites containing dMHC+ fibers **(G–J)**. Scale bars = 20 μm. Histogram showing increased numbers of CD68+ macrophages located at sites of dMHC+ regenerative areas relative to dMHC- areas in muscles of WT/*mdx* and LIF/*mdx* mice **(K)**. * indicates significant difference between the two groups indicated by the ends of the horizontal brackets ($P < 0.05$). *P*-values are based on two-tailed t-test for all groups. $N = 5$ for all groups. Bars = SEM.

may underlie the reduction in monocyte/macrophage recruitment and dispersion in LIF/*mdx* muscles.

The reduction in numbers of CD206+ macrophages, an M2-biased phenotype that can promote muscle fibrosis and regener-

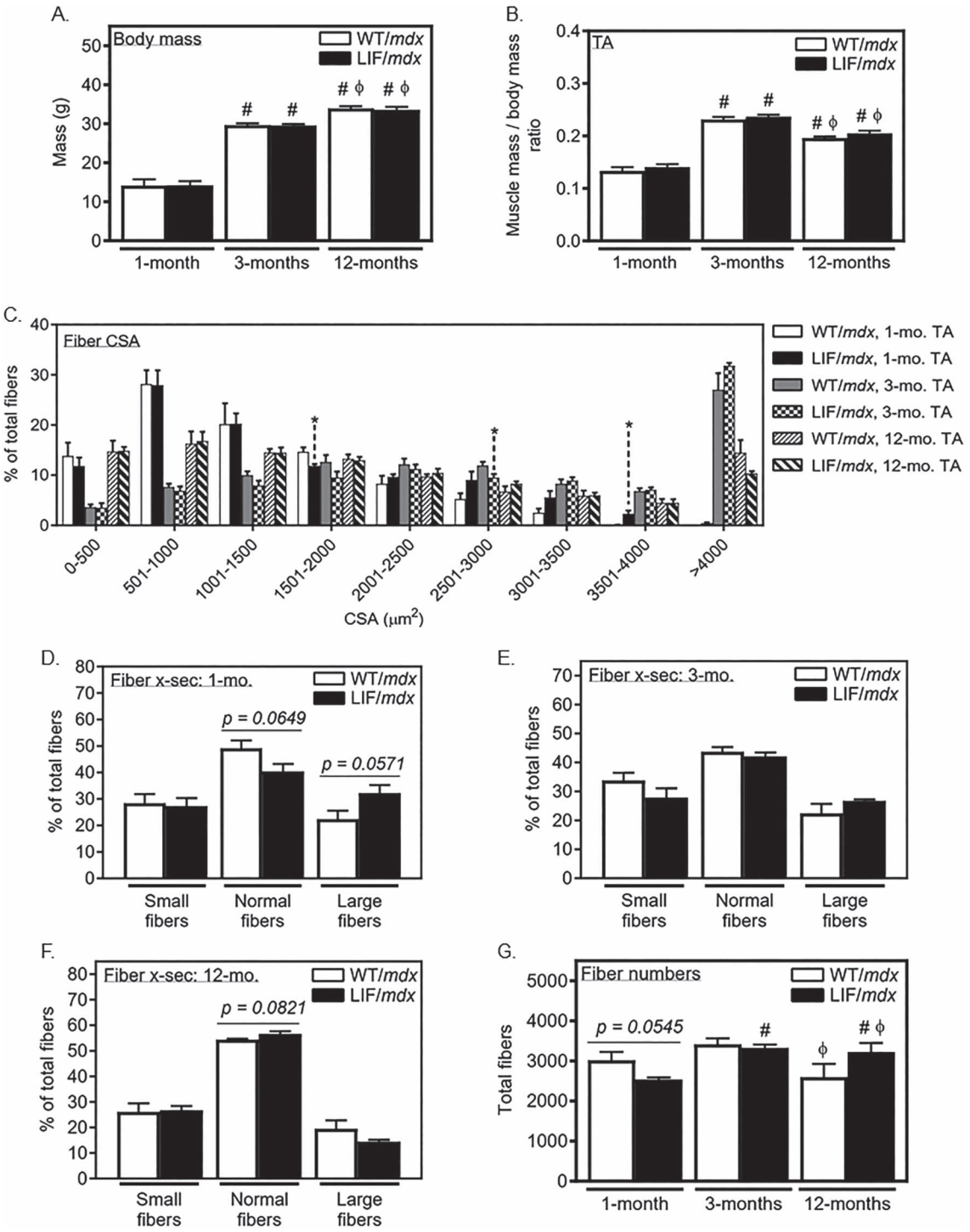

Figure 8. The transgene has little influence on muscle fiber size or growth. Measurements of body mass **(A)**, TA muscle mass to body mass ratio **(B)**, fiber CSA **(C–F)** and fiber numbers **(G)** show no significant difference between WT/*mdx* and LIF/*mdx* mice. * indicates significant difference compared to age-matched, WT/*mdx* mice at the same CSA bin ($P < 0.05$). # and Φ indicate significant difference compared to 1- and 3-month mice of the same genotype, respectively. *P*-values are based on two-tailed t-tests. *N* = at least 6 for all groups shown in each data graph. Bars = SEM.

ation (18,19,22,65), indicates that elevated expression of LIF may influence macrophage phenotype, shifting them toward a pro-inflammatory, cytolytic M1-biased phenotype. That possibility is supported by previous findings which showed that elevated expression of LIF in inflammatory cells in *mdx* muscles reduced the expression of IL-4 and IL-10 (1), which can be produced by M2-biased macrophages and promote the M2 phenotype (21–23,29,30,32,34,35). However, this differs from the role of LIF in regulating macrophage phenotype in some other diseases. For example, blockade of LIF signaling in tumors in which LIF is expressed at high levels produced a reduction in the expression of M2 phenotypic markers in tumor-associated macrophages,

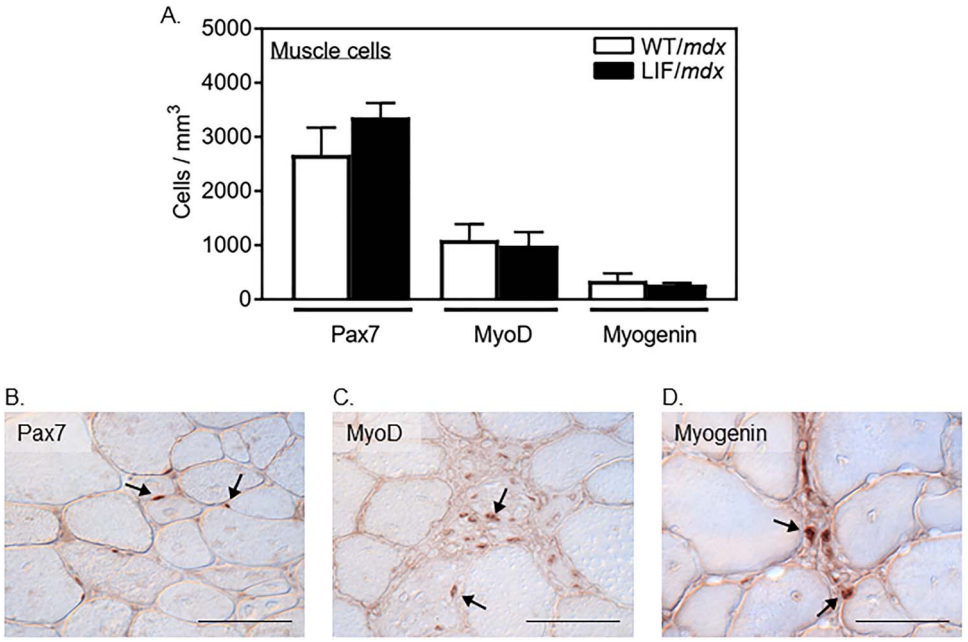

Figure 9. CD11b/LIF expression does not affect myogenesis in dystrophic muscle. Numbers of muscle cells expressing Pax7, MyoD or myogenin are unaffected by transgene expression in the muscles of *mdx* mice **(A)** ($P < 0.05$). *P*-values are based on two-tailed t-tests. $N = 4$ for all groups except WT/*mdx* mice used to quantify MyoD+ cells ($n = 5$). Bars = SEM. Representative images of Pax7+ **(B)**, MyoD+ **(C)** and myogenin+ **(D)** cells in LIF/*mdx* muscles. Examples of positively labeled cells are indicated with arrows. Scale bars = 50 μm.

including CD206 and CD163 (66). In addition, peripheral blood monocytes from human donors that were directly stimulated with LIF *in vitro* exhibited an M2-biased phenotype (17).

Our finding that expression of the CD11b/LIF transgene did not amplify the number of satellite cells in *mdx* muscles contrasts with previous observations which showed that LIF could increase numbers of C2C12 myoblasts *in vitro* by increasing their proliferation, reducing their apoptosis and delaying their differentiation into post-mitotic myotubes (3,4,6,7,67). However, whether elevations in LIF delivery to injured or diseased muscle affects satellite cell numbers *in vivo* has not been previously tested. The lack of effect of CD11b/LIF transgene expression on satellite cell numbers is therapeutically relevant because reductions in satellite cell numbers over the course of *mdx* muscular dystrophy contribute significantly to the decline of regenerative potential of dystrophic muscle (68–71). Similarly, expression of the CD11b/LIF transgene did not affect muscle fiber size in *mdx* mice. This differs from the increase in *mdx* muscle fiber size that resulted from suturing alginate rods that were infused with recombinant LIF to dystrophic muscles, allowing LIF to diffuse into the muscle for 3 months, leading to an increase in muscle fiber size (12). These differing treatment outcomes may reflect differences in the concentration, location and timing of LIF delivery to the *mdx* muscles, as indicated in investigations of the effects of LIF administration to acutely injured muscle. For example, continuous delivery of recombinant LIF to acutely injured muscle by a mini-osmotic pump increased muscle fiber growth (9) but systemic elevations of recombinant LIF using three intraperitoneal injections per week did not affect the growth of muscle fibers following acute injury (72).

Collectively, our current findings and previous work (1) show that the therapeutic value of inflammatory cell-mediated delivery of a CD11b/LIF transgene to dystrophic muscle may result primarily from its reduction of muscle fibrosis, and not from improving the growth or regenerative capacity of dystrophic muscle. Expression of the transgene produced long-term reductions in the expression and accumulation of connective tissue proteins in dystrophic muscle (1), which diminished muscle stiffness, which is a debilitating feature of muscular dystrophy (73–75). However, the potential for expression of the transgene to cause transient increases in muscle fiber damage early in the pathology, while reducing damage at later stages, indicates that this therapeutic approach would be best administered at later stages of the pathology, when progressive fibrosis is a prominent feature of the disease.

Materials and methods

Mice

All experimentation complied with relevant ethical regulations for animal testing and research, and experimental study protocols were approved by the Chancellor's Animal Research Committee at the University of California, Los Angeles. C57BL/10ScSn-Dmd*mdx*/J mice (*mdx* mice) were purchased from The Jackson Laboratory (Bar Harbor, ME) and bred in specific pathogen-free vivaria.

The CD11b/LIF *mdx* mouse line was generated using the following strategy. The complete *Mus musculus* LIF cDNA sequence (611-bp; NM_008501) was amplified by PCR and ligated into a pGL3-Basic vector (Promega) at the Nco I/Xba I sites. The pGL3-Basic vector also contained a 550-bp fragment of the human CD11b promoter at the Hind III site, upstream of the LIF insertion site. The 1215-bp, hCD11b/LIF fragment was isolated from pGL3-Basic by restriction endonuclease digestion with Xho I/Xba I and used for pronuclear injection into CB6F1 eggs to generate transgenic mice. Positive founders were identified by PCR screening for the hCD11b/LIF construct. Founder mice were backcrossed with C57BL/6 J mice for at least seven generations to generate hemizygous, transgenic (CD11b/LIF.Tg+) mice.

CD11b/LIF *mdx* transgenic mice were produced by crossing CD11b/LIF.Tg+, hemizygous males with *mdx* females to generate CD11b/LIF.Tg+ hemizygous, transgenic mice that were dystrophin-deficient. Dystrophin deficiency was verified by ARMS PCR screening and presence of the hCD11b/LIF construct was determined by PCR screening. The CD11b/LIF *mdx* mice were backcrossed with wild-type *mdx* mice for seven generations to produce hemizygous CD11b/LIF *mdx* mice. The CD11b/LIF *mdx* line is maintained as hemizygous to produce transgenic (LIF/*mdx*) mice and wild-type (WT/*mdx*) littermate controls for experimentation. We showed in previous work that muscle tissue from this transgenic mouse line has more than 60% greater expression of LIF than WT/*mdx* mice (1).

LIF/*mdx* and WT/*mdx* mice were euthanized by inhalation of 32% isoflurane (Zoetis) at 1-, 3- or 12-months of age. Body mass was recorded prior to tissue collection. Both tibialis anterior (TA) muscles were dissected from each mouse and the individual muscle masses were recorded. Investigators collecting data and performing analysis were aware of animal numbers only and were blinded to treatment groups.

Immunohistochemistry

The right TA muscle from each male mouse was dissected and immediately frozen in O.C.T. compound (Tissue-Tek) in liquid nitrogen-cooled isopentane. Muscle cross-sections were cut at a thickness of 10 μm at −20°C and mounted onto glass slides. Cross-sections were fixed for 10 min in acetone cooled to −80°C (for sections to be labeled with anti-CD11b, anti-CD206, anti-CD68, anti-developmental myosin heavy chain (dMHC) or anti-MyoD) or 2% paraformaldehyde (PFA) cooled to 4°C (for sections to be labeled with anti-LIF) or 4% PFA cooled to 4°C (for sections to be labeled with anti-Pax7 or anti-myogenin), or methanol cooled to 4°C (for sections to be labeled with anti-albumin). Endogenous peroxidase activity was quenched using 0.3% H_2O_2 for 10 min. Sections to be labeled for Pax7, MyoD and myogenin were immersed in antigen retrieval buffer (10 mM sodium citrate, 0.05% Tween-20, pH 6) at 95–100°C for 40 min prior to the peroxidase quench step. Sections to be labeled with anti-CD11b, anti-CD206 or anti-CD68 were blocked at room temperature (RT) in bovine serum albumin (BSA) buffer (3% BSA, 0.05% Tween-20, 0.2% gelatin, 0.15 M NaCl, 0.05 M Tris–HCl; 30 min). Sections to be labeled with anti-LIF were blocked in 3% ovalbumin buffer (3% ovalbumin, 0.05% Tween-20, 0.2% gelatin, 0.15 M NaCl, 0.05 M Tris–HCl; 30 min). Sections to be labeled with anti-Pax7, anti-MyoD or anti-myogenin were blocked with M.O.M. blocking buffer (Vector #PK-2200). Sections to be labeled with anti-albumin were blocked with 1% gelatin buffer (1% gelatin, 0.05% Tween-20, 0.15 M NaCl, 0.05 M Tris–HCl; 45 min). Sections were then incubated with rat anti-CD11b (1:100; overnight at 4°C; BioLegend #101202), rat anti-CD68 (1:100; 3 h at RT; AbD Serotec #MCA1957), rat anti-CD206 (1:50; 3 h at RT; AbD Serotec #MCA2235), goat anti-LIF (1:66; overnight at 4°C; R&D Systems #AB-449), rabbit anti-albumin (1:20; overnight at 4°C; Accurate Chemical #YNRRAALBP), mouse anti-dMHC (1:100; overnight at 4°C; Novocastra #NCL-MHCd), mouse anti-Pax7 (1:300; overnight at 4°; Developmental Studies Hybridoma Bank), mouse anti-MyoD (1:50; overnight at 4°C; BD Pharmingen #554130) or mouse anti-myogenin (1:50; overnight at 4°C; BD Pharmingen #556358). The sections were incubated with an appropriate biotinylated secondary antibody for 30 min at RT and then incubated with avidin D-conjugated horseradish peroxidase (1:1000; 30 min at RT; Vector #A-2004). The blocking reagent, secondary antibody and peroxidase reagent used for sections labeled for anti-dMHC, anti-Pax7, anti-MyoD and anti-myogenin were part of a M.O.M. detection kit (Vector #PK-2200). Positive signal was visualized in all slides with the peroxidase substrate, 3-amino-9-ethylcarbazole (AEC, Vector #SK-4200). The sections were washed in phosphate buffered saline (PBS) after each step, beginning with the fixation.

Stereology

The number of cells per volume of muscle was determined by measuring the total volume of each section using a stereological, point-counting technique to determine section area and then multiplying that value by the section thickness (10 μm). The numbers of immunolabeled cells in each section were counted and expressed as the number of cells per volume of each section ([total cells]/[mm^3]). Cell counts were performed on an Olympus BX50 microscope equipped with Nomarski optics.

Immunofluorescence

Macrophages expressing CCL2 were identified in tissue sections that were fixed in acetone cooled to −80°C. The sections were first blocked in 3% ovalbumin buffer for 30 min. The sections were then incubated with rat anti-F4/80 (1:50; Affimatrix eBioscience #14–8011) and goat anti-CCL2 (1:75; R&D Systems #AB-479-NA) overnight at 4°C and then incubated with a biotinylated anti-goat secondary antibody (1:200; Vector BA-9500) for 30 min at RT. The sections were then incubated with anti-rat fluorescent secondary antibody (1:200; DyLight 488; Abcam #ab102260) and DyLight 594 streptavidin (1:300; Vector SA-5594) in PBS for 30 min at RT before mounting with ProLong Gold mounting medium with DAPI (ThermoFisher Scientific #P36931). The sections were washed in PBS after each step, beginning with the fixation. The data were expressed as the proportion of F4/80+ macrophages that were also CCL2+ out of the total F4/80+ macrophage population ([F4/80+CCL2+ cells]/[total F4/80+ cells]). Cell counts were performed on a Leica DMRXA fluorescence microscope. Confocal images were acquired on a Leica TCS-SP5 confocal microscope.

The distribution of CD68+ macrophages relative to sites in muscle that were enriched in dMHC+ fiber was assayed in muscle sections following fixation in acetone cooled to −80°C. The sections were blocked in M.O.M. blocking buffer (Vector #PK-2200) for 1 h at RT. The sections were then incubated in rat anti-CD68 (1:100; Serotec #MCA 1957) and mouse anti-dMHC (1:100; Novocastra #NHC-MHCd) overnight at 4°C in M.O.M. protein dilute (Vector #PK-2200). The sections were incubated with anti-rat (1:200; DyLight 488; Abcam #ab102260) and anti-mouse (1:200; DyLight 594; Vector #DI-2594) fluorescent antibodies for 30 min at RT before mounting with ProLong Gold Mounting medium with DAPI. The sections were washed in PBS following each step of their processing. Data were collected by identifying sites containing dMHC+ fibers and then counting the numbers of CD68+ macrophages in a standardized volume of 289 000 μm^3 surrounding the dMHC+ fibers. The volume utilized was calculated using a point-counting technique to calculate the area of the field of view surrounding dMHC+ sites (28 900 μm^2) and multiplying the area by the section thickness (10 μm). All sites containing dMHC+ fibers in each sample were used for data collection. An equivalent number of healthy sites of equal volume were used to quantify the numbers of CD68+ macrophages at sites without dMHC+ fibers in each sample. The data were expressed as the density of CD68+ cells per mm^3 (CD68+ cells/mm^3). Cell counts were performed on an Olympus

Table 1.

Gene	Forward	Reverse
tpt1	GGAGGGCAAGATGGTCAGTAG	CGGTGACTACTGTGCTTTCG
rnps1	AGGCTCACCAGGAATGTGAC	CTTGGCCATCAATTTGTCCT
hprt1	GCTGACCTGCTGGATTACATTAAAG	CCACCAATAACTTTTATGTCCCC
lif	GTCTTGGCCGCAGGGATTG	GCACAGGTGGCATTTACAGG
ccl2	GCTCAGCCAGATGCAGTTAAC	CTCTCTCTTGAGCTTGGTGAC

BH2 fluorescence microscope. Confocal images were acquired on a Leica TCS-SP5 confocal microscope.

The relative quantity of LIF in LIF/*mdx* and WT/*mdx* muscle fibers was assayed by determining the mean fluorescence intensity (MFI) of muscle fibers following labeling with anti-LIF and a fluorescent secondary antibody. Sections were fixed in 2% PFA cooled to 4°C. PFA-induced autofluorescence was quenched by submerging the sections in 0.1 M glycine in PBS for 5 min. The sections were incubated with goat anti-LIF (1:66; R&D Systems #AB-449) overnight at 4°C. The sections were then incubated with a biotinylated anti-goat secondary antibody (1:200; Vector #BA-9500) for 30 min at RT. The sections were incubated with a fluorophore-conjugated streptavidin (1:300; DyLight 594; Vector #SA-5594) for 30 min at RT before mounting with ProLong Gold Mounting medium with DAPI. The sections were washed in PBS after each step. The MFI of 20 randomly selected muscle fibers in each sample was quantified using ImageJ (National Institutes of Health). Images used for MFI measurements were acquired on an Olympus BH2 fluorescence microscope. Confocal images were acquired on a Leica TCS-SP5 confocal microscope.

Myofiber number quantification and CSA measurements

Cross-sections from the TA muscle mid-belly were stained with hematoxylin (Vector #H-3401) for 10 min. Muscle fiber CSA was quantified using ImageJ (National Institutes of Health). The average CSA of each sample was calculated from 500 randomly sampled fibers. The classification for large or small fibers was determined by setting three standard deviations from the mean CSA for the control group at each time-point as previously described (76). Fibers were considered to be small or large in 1-month TAs if the CSA was less than 796 μm^2 or greater than 1785 μm^2, respectively. Fibers were considered to be small or large in 3-month TAs if the CSA was less than 2000 μm^2 or greater than 4414 μm^2, respectively. Fibers were considered to be small or large in 12-month TAs if the CSA was less than 832 μm^2 or greater than 3453 μm^2, respectively. Fibers were considered normal if their CSA was between the threshold measurements for small and large fibers. Images used for CSA measurements were acquired on an Olympus BH2 microscope equipped with Nomarski optics.

RNA isolation and quantitative PCR

Cell cultures were washed with Dulbecco's phosphate-buffered saline (DPBS, Sigma-Aldrich #5652) cooled to 4°C and the RNA was isolated in TRIzol Reagent (Ambion #15596018) according to the manufacturer's protocol. The isolated RNA was further cleaned and concentrated using an RNA Clean and Concentrator-5 kit (Zymo Research #R1014). The RNA was quantified, reversed transcribed to cDNA, and used for qPCR as previously described (18,77). We followed established guidelines for experimental design, data normalization and data analysis (78–80). Primer sequences used for qPCR are listed in Table 1.

Muscle macrophage isolation

Skeletal muscles from male and female, 1-month-old *mdx* mice were minced in 1.25 mg/ml collagenase types IA and IV (Sigma-Aldrich #C9891, #C5138) in Dulbecco's Modified Eagle medium (Sigma #D1152) and digested at 37°C for 1 h with gentle trituration each 15 min. The digestate was diluted with DPBS, filtered through 70 μm mesh filters and the liberated cells collected by centrifugation. The cells were resuspended in DPBS, overlaid on Histopaque-1077 (Sigma-Aldrich #1077-1) and centrifuged at 400 x g for 30 min at RT. Macrophages were collected from the DPBS-Histopaque interface and RNA isolated from the cells as described above. QPCR was performed using *tpt1* and *hprt1* as house-keeping genes. Muscle macrophages were collected from five WT/*mdx* and three LIF/*mdx* mice.

Preparation of BMDMs for RNA analysis

BMCs were aseptically flushed from femurs and tibiae with DPBS and treated with ACK lysis buffer (Lonza #10-548E) to lyse red blood cells. BMCs from three male mice of the same genotype were pooled together to generate CD11b/LIF- and CD11b/LIF+ BMDMs. Following a wash with DPBS and filtration through a 70 μm mesh filter, the BMCs were plated in 6-cm tissue culture dishes (1×10^7 cells/dish) in macrophage growth medium (RPMI-1640 (Sigma #R6504), 20% heat-inactivated fetal bovine serum (HI-FBS, Omega Scientific #FB-11), 100 U/ml penicillin +100 μg/ml streptomycin (1% Pen/Strep, Gibco #15140-122), 10 ng/ml macrophage colony-stimulating factor (M-CSF, Cell Applications Inc. #RP2008)) at 37°C in 5% CO_2 for 6 days. The macrophage growth medium was replenished on days 3 and 5 post-plating. On day 6, adherent cells were activated to an M1-biased or M2-biased phenotype in macrophage activation medium (DMEM (Sigma-Aldrich #D1152), 0.25% HI-FBS, 1% Pen/Strep, 10 ng/ml M-CSF and either Th1 cytokines (10 ng/ml IFNγ and 10 ng/ml TNFα; BD Pharmingen #554587 and 554 589) or Th2 cytokines (25 ng/ml IL-4 and 10 ng/ml IL-10; BD Pharmingen #550067 and 550 070)) for 48 h. The activation medium was replenished after the first 24 h of activation. Th0 BMDMs were generated by culturing the adherent cells in macrophage activation medium without Th1 or Th2 cytokines. RNA from the cells was isolated as described above. QPCR was performed using *tpt1* and *rnps1* as house-keeping genes.

ELISA analysis of CCL2 in BMDM conditioned media

CCL2 secretion by BMDMs was measured as previously described (1). Briefly, BMDMs from wild-type, WT/*mdx* and LIF/*mdx* mice were generated as described above. BMCs from two male mice of each genotype were pooled to generate the BMDMs. On the sixth day of culture, the BMDMs were switched to DMEM containing

0.25% HI-FBS, 1% Pen/Strep and 10 ng/ml M-CSF, with or without 10 ng/ml recombinant mouse LIF (eBioscience #14-8521). After 24 h of stimulation, the conditioned media were collected, briefly centrifuged to remove particulates, and analyzed for BMDM-secreted CCL2 (Duoset ELISA, R&D Systems, #DY479) according to the manufacturer's instructions.

Cytotoxicity assay

Macrophage-mediated cytotoxicity was assessed using co-cultures of BMDMs and C2C12 muscle cells. BMDMs from one female mouse of each genotype (WT/*mdx* and LIF/*mdx*) were generated as described above with the following modifications. Freshly isolated BMCs were plated at 5×10^6 cells per 10-cm, low-adherence dish (Eisco #CH0372C) in macrophage growth medium for 6 days. Adherent cells were activated to a cytotoxic, M1-biased phenotype using activation medium containing Th1 cytokines for 24 h. Unstimulated BMDMs were cultured in activation medium without Th1 cytokines. Following activation, the BMDMs were washed with DPBS and detached from the dishes using Cellstripper (Corning #25-056-Cl) for 10 min. The detached BMDMs were centrifuged at 526 x g for 5 min, resuspended in DPBS, and total cell numbers were calculated using a hemocytometer. BMDMs were resuspended in cytotoxicity assay medium (Hank's balanced salt solution (HBSS; Sigma-Aldrich #H1387), 0.25% HI-FBS, 400 μM L-arginine).

One day prior to co-culture, 12-well plates were prepared by adding 8-mm glass coverslips coated with 2% gelatin to each well. C2C12 muscle cells were plated in the 12-well plates at 5.94×10^4 cells per well in growth medium (DMEM (Sigma-Aldrich #D1152), 10% FBS, 1% Pen/Strep) for 24 h to allow the cells to reach 70% confluency and attach to the glass coverslips. The muscle cells were then washed with DPBS and fluorescently labeled with CFDA-SE (Accurate Chemical #14456) to allow visual differentiation from unlabeled BMDMs. The muscle cells were incubated in labeling medium (HBSS, 0.1% BSA, 5 μM CFDA-SE) for 10 min at 37°C in 5% CO_2. CFDA-SE is a cell membrane-permeable dye that does not cause cytotoxicity at the concentration used. Intracellular CFDA-SE is cleaved by endogenous esterases to form cell membrane-impermeable CFSE. CFSE is a fluorescent molecule (488 nm emission) that binds intracellular proteins, permanently labeling cells. The cells were washed with growth medium to remove residual CFDA-SE from each well. The cells were then incubated in growth medium for 5 min at 37°C in 5% CO_2 to allow unreacted CFDA-SE to flow out of the cells and avoid labeling BMDMs. The labeled cells received a final wash using HBSS to remove residual growth medium.

The BMDMs were added to the muscle cultures at 1.3×10^6 BMDMs/well in cytotoxicity assay medium. Following 6 h of co-culture at 37°C in 5% CO_2, each co-culture well was washed with DPBS. GelRed (Biotium #41003-1) diluted in cytotoxicity assay medium (1:2500 dilution) was added to each well for 10 min at 37°C in 5% CO_2 to label permeabilized muscle cells. GelRed is a cell membrane-impermeable, fluorescent dye (593 nm emission) that binds to nucleic acids. Following a final DPBS wash, the glass coverslips were removed from each well and mounted onto glass microscope slides using Fluoro-Gel (Electron Microscopy Sciences #17985-10).

Fluorescence microscopy with an Olympus BH2 microscope was used to collect cytotoxicity data based on the following criteria: BMDMs were CFSE-GelRed-, non-permeabilized muscle cells were CFSE+GelRed- and permeabilized muscle cells were CFSE+GelRed+. Data were expressed as the proportion of permeabilized muscle cells out of total C2C12 cells ([CFSE+GelRed+ cells]/[total CFSE+ cells]) on each coverslip. Three coverslips were included per group. The proportion of permeabilized muscle cells was quantified from 15 randomly chosen fields per coverslip. The average proportion of permeabilized muscle cells per coverslip was calculated and used as a single datum to calculate the mean and SEM for each group. The data were normalized to a muscle cell-only control group. Data were verified by repeating the experiment in triplicate.

In a separate experiment, we verified the sensitivity of this assay by testing the influence of increasing numbers of Th1-stimulated BMDMs on muscle cell lysis. The experiment was repeated as described above. The muscle cell cultures were co-cultured with no BMDMs, low numbers of BMDMs (6.55×10^5 cells), medium numbers of BMDMs (1.30×10^6 cells) or high numbers of BMDMs (2.60×10^6 cells). Because the wells containing high numbers of BMDMs prevented accurate counts of total muscle cells, data were expressed as GelRed+ cells/mm^2.

Chemotaxis assay

BMDMs were isolated from two male mice of each genotype (WT/*mdx* and LIF/*mdx*) using the following strategy. BMCs were aseptically flushed from the femurs and tibiae as described earlier. The BMCs were plated at 1.0×10^7 cells per 6-cm, ultra-low attachment dish (Corning #3261) in macrophage growth medium containing Th1 or Th2 cytokines for 24 h at 37°C in 5% CO_2. Unpolarized BMDMs were cultured in macrophage growth medium without additional cytokines. The cells were washed with DPBS and adherent cells were detached using Cellstripper as described previously. The cells were collected and BMDMs were purified using a Histopaque-1077 gradient (Sigma-Aldrich #10771) according to the manufacturer's instructions. The BMDMs were resuspended in chemotaxis medium (RPMI-1640, 1% Pen/Strept, 1% BSA).

We tested the chemotactic ability of the BMDMs in response to CCL2 using a chemotaxis chamber (Neuro Probe #AP48) following the manufacturer's protocol. We used 10 ng/ml of CCL2 (R&D Systems #479-JE/CF) in chemotaxis medium to measure chemotaxis. Spontaneous migration was measured using chemotaxis medium without CCL2. Cells in the chemotaxis chamber were incubated for 2 h at 37°C in 5% CO_2.

Three wells were included in each group. The numbers of migratory cells were quantified in five randomly chosen fields per well. The average number of migratory cells per field in each well was calculated and used as a single datum to calculate the mean and SEM for each group. Data were verified by repeating the experiment in triplicate. Data were collected using an Olympus BX50 microscope equipped with Nomarski optics.

Statistical analysis

All data are presented as mean ± SEM. Statistical significance was calculated using an unpaired Student's t-test, one-way analysis of variance (ANOVA) with Tukey's multiple comparisons test, or two-way ANOVA with Tukey's multiple comparisons test using Prism 7 (GraphPad). Differences with a P-value < 0.05 were considered statistically significant.

Supplementary Material

Supplementary Material is available at *HMG* online.

Acknowledgements

Confocal laser scanning microscopy was performed at the California NanoSystems Institute Advanced Light Microscopy-/Spectroscopy Shared Resource Facility at UCLA. DNA microinjections for the production of the CD11b/LIF transgenic mice were performed at the University of California, Irvine Transgenic Mouse Facility. The Pax7 hybridoma developed by T.M. Jessell, Columbia University, was obtained from the Developmental Studies Hybridoma Bank, created by the NICHD of the NIH and maintained at The University of Iowa, Department of Biology, Iowa City, IA 52242.

Conflict of Interest statement. The authors have no competing interests to declare.

Funding

This work was supported by the National Institute of Arthritis and Musculoskeletal and Skin Diseases of the National Institutes of Health under award numbers F31AR071783 (to IF), F32AR065845 (to SSW) and RO1AR066036, RO1AR062579 and R21AR066817 (to JGT).

References

1. Welc, S.S., Flores, I., Wehling-Henricks, M., Ramos, J., Wang, Y., Bertoni, C. and Tidball, J.G. (2019) Targeting a therapeutic LIF transgene to muscle via the immune system ameliorates muscular dystrophy. *Nat. Commun.*, **10**, 1–17.
2. Dadgar, S., Wang, Z., Johnston, H., Kesari, A., Nagaraju, K., Chen, Y., Hill, D.A., Partridge, T.A., Giri, M., Freishtart, R.J. *et al.* (2014) Asynchronous remodeling is a driver of failed regeneration in Duchenne muscular dystrophy. *J. Cell Biol.*, **207**, 139–158.
3. Austin, L. and Burgess, A.W. (1991) Stimulation of myoblast proliferation in culture by leukaemia inhibitory factor and other cytokines. *J. Neurol. Sci.*, **101**, 193–197.
4. Austin, L., Bower, J., Kurek, J. and Vakakis, N. (1992) Effects of leukaemia inhibitory factor and other cytokines on murine and human myoblast proliferation. *J. Neurol. Sci.*, **112**, 185–191.
5. Broholm, C., Laye, M.J., Brandt, C., Vadalasetty, R., Pilegaard, H., Pedersen, B.K. and Scheele, C. (2011) LIF is a contraction-induced myokine stimulating human myocyte proliferation. *J. Appl. Phys.*, **111**, 251–259.
6. Spangenburg, E.E. and Booth, F.W. (2002) Multiple signaling pathways mediate LIF-induced skeletal muscle satellite cell proliferation. *Am. J. Physiol. Cell Physiol.*, **283**, C204–C211.
7. Hunt, L.C., Upadhyay, A., Jazayeri, J.A., Tudor, E.M. and White, J.D. (2011) Caspase-3, myogenic transcription factors and cell cycle inhibitors are regulated by leukemia inhibitory factor to mediate inhibition of myogenic differentiation. *Skelet. Muscle*, **1**, 17.
8. Gao, S., Durstine, J.L., Koh, H.-J., Carver, W.E., Frizzell, N. and Carson, J.A. (2017) Acute myotube protein synthesis regulation by IL-6-related cytokines. *Am. J. Physiol. Cell Physiol.*, **313**, C487–C500.
9. Barnard, W., Bower, J., Brown, M.A., Murphy, M. and Austin, L. (1994) Leukemia inhibitory factor (LIF) infusion stimulates skeletal muscle regeneration after injury: injured muscle expresses lif mRNA. *J. Neurol. Sci.*, **123**, 108–113.
10. Finkelstein, D.I., Bartlett, P.F., Horne, M.K. and Cheema, S.S. (1996) Leukemia inhibitory factor is a myotrophic and neurotrophic agent that enhances the reinnervation of muscle in the rat. *J. Neurosci. Res.*, **46**, 122–128.
11. Kurek, J.B., Bower, J.J., Romanella, M., Koentgen, F., Murphy, M. and Austin, L. (1997) The role of leukemia inhibitory factor in skeletal muscle regeneration. *Muscle Nerve*, **20**, 815–822.
12. Austin, L., Bower, J.J., Bennett, T.M., Lynch, G.S., Kapsa, R., White, J.D., Barnard, W., Gregorevic, P. and Byrne, E. (2000) Leukemia inhibitory factor ameliorates muscle fiber degeneration in the mdx mouse. *Muscle Nerve*, **23**, 1700–1705.
13. Mori, M., Yamaguchi, K., Honda, S., Nagasaki, K., Ueda, M., Abe, O. and Abe, K. (1991) Cancer cachexia syndrome developed in nude mice bearing melanoma cells producing leukemia-inhibitory factor. *Cancer Res.*, **51**, 6656–6659.
14. Tisdale, M.J. (2002) Cachexia in cancer patients. *Nat. Rev. Cancer*, **2**, 862–871.
15. Seto, D.N., Kandarian, S.C. and Jackman, R.W. (2015) A key role for leukemia inhibitory factor in C26 cancer cachexia. *J. Biol. Chem.*, **290**, 19976–19986.
16. Hunt, L.C., Upadhyay, A., Jazayeri, J.A., Tudor, E.M. and White, J.D. (2013) An anti-inflammatory role for leukemia inhibitory factor receptor signaling in regenerating skeletal muscle. *Histochem. Cell Biol.*, **139**, 13–34.
17. Duluc, D., Delneste, Y., Tan, F., Moles, M., Grimaud, L., Lenoir, J., Preisser, L., Anegon, I., Catala, L., Ifrah, N. *et al.* (2007) Tumor-associated leukemia inhibitory factor and IL-6 skew monocyte differentiation into tumor-associated macrophage-like cells. *Blood*, **110**, 4319–4330.
18. Villalta, S.A., Deng, B., Rinaldi, C., Wehling-Henricks, M. and Tidball, J.G. (2011) IFN-γ promotes muscle damage in the mdx mouse model of Duchenne muscular dystrophy by suppressing M2 macrophage activation and inhibiting muscle cell proliferation. *J. Immunol.*, **187**, 5419–5428.
19. Wehling-Henricks, M., Jordan, M.C., Gotoh, T., Grody, W.W., Roos, K.P. and Tidball, J.G. (2010) Arginine metabolism by macrophages promotes cardiac and muscle fibrosis in mdx muscular dystrophy. *PLoS One*, **5**, e10763.
20. Deng, B., Wehling-Henricks, M., Villalta, S.A., Wang, Y. and Tidball, J.G. (2012) IL-10 triggers changes in macrophage phenotype that promote muscle growth and regeneration. *J. Immunol.*, **189**, 3669–3680.
21. Welc, S.S., Wehling-Henricks, M., Antoun, J., Ha, T.T., Tous, I. and Tidball, J.G. (2020) Differential effects of myeloid cell PPARδ and IL-10 in regulating macrophage recruitment, phenotype, and regeneration following acute muscle injury. *J. Immunol.*, **205**, 1664–1677.
22. Villalta, S.A., Nguyen, H.X., Deng, B., Gotoh, T. and Tidball, J.G. (2009) Shifts in macrophage phenotypes and macrophage competition for arginine metabolism affect the severity of muscle pathology in muscular dystrophy. *Hum. Mol. Genet.*, **18**, 482–496.
23. Villalta, S.A., Rinaldi, C., Deng, B., Liu, G., Fedor, B. and Tidball, J.G. (2011) Interleukin-10 reduces the pathology of mdx muscular dystrophy by deactivating M1 macrophages and modulating macrophage phenotype. *Hum. Mol. Genet.*, **20**, 790–805.
24. Wehling-Henricks, M., Lee, J.J. and Tidball, J.G. (2004) Prednisolone decreases cellular adhesion molecules required for inflammatory cell infiltration in dystrophin-deficient skeletal muscle. *Neuromuscul. Disord.*, **14**, 483–490.
25. Nguyen, H.X., Lusis, A.J. and Tidball, J.G. (2005) Null mutation of myeloperoxidase in mice prevents mechanical activation

of neutrophil lysis of muscle cell membranes in vitro and in vivo. *J. Physiol.*, **565**, 403–413.
26. Wehling-Henricks, M., Sokolow, S., Lee, J.J., Myung, K.H., Villalta, S.A. and Tidball, J.G. (2008) Major basic protein-1 promotes fibrosis of dystrophic muscle and attenuates the cellular immune response in muscular dystrophy. *Hum. Mol. Genet.*, **17**, 2280–2292.
27. Tidball, J.G. and Villalta, S.A. (2010) Regulatory interactions between muscle and the immune system during muscle regeneration. *Am. J. Physiol. Regul. Integr. Comp. Physiol.*, **298**, R1173–R1187.
28. Locati, M., Mantovani, A. and Sica, A. (2013) Macrophage activation and polarization as an adaptive component of innate immunity. *Adv. Immunol.*, **120**, 163–184.
29. Murray, P.J., Allen, J.E., Biswas, S.K., Fisher, E.A., Gilroy, D.W., Goerdt, S., Gordon, S., Hamilton, J.A., Ivashkiv, L.B., Lawrence, T. *et al.* (2014) Macrophage activation and polarization: nomenclature and experimental guidelines. *Immunity*, **41**, 14–20.
30. Mills, C.D., Kincaid, K., Alt, J.M., Heilman, M.J. and Hill, A.M. (2000) M-1/M-2 Macrophages and the Th1/Th2 paradigm. *J. Immunol.*, **164**, 6166–6173.
31. Tidball, J.G. (2017) Regulation of muscle growth and regeneration by the immune system. *Nat. Rev. Immunol.*, **17**, 165–178.
32. Lang, R., Patel, D., Morris, J.J., Rutschman, R.L. and Murray, P.J. (2002) Shaping gene expression in activated and resting primary macrophages by IL-10. *J. Immunol.*, **169**, 2253–2263.
33. Mosser, D.M. (2003) The many faces of macrophage activation. *J. Leukoc. Biol.*, **73**, 209–212.
34. Mosser, D.M. and Zhang, X. (2008) Interleukin-10: new perspectives on an old cytokine. *Immunol. Rev.*, **226**, 205–218.
35. Martinez-Pomares, L., Reid, D.M., Brown, G.D., Taylor, P.R., Stillion, R.J., Linehan, S.A., Zamze, S., Gordon, S. and Wong, S.Y.C. (2003) Analysis of mannose receptor regulation by IL-4, IL-10, and proteolytic processing using novel monoclonal antibodies. *J. Leukoc. Biol.*, **73**, 604–613.
36. Hakim, C.H., Grange, R.W. and Duan, D. (2011) The passive mechanical properties of the extensor digitorum longus muscle are compromised in 2- to 20-mo-old mdx mice. *J. Appl. Physiol.*, **110**, 1656–1663.
37. Hourdé, C., Joanne, P., Noirez, P., Agbulut, O., Butler-Browne, G. and Ferry, A. (2013) Protective effect of female gender–related factors on muscle force-generating capacity and fragility in the dystrophic mdx mouse. *Muscle Nerve*, **48**, 68–75.
38. Wehling-Henricks, M., Li, Z., Lindsey, C., Wang, Y., Welc, S.S., Ramos, J.N., Khanlou, N., Kuro-o, M. and Tidball, J.G. (2016) Klotho gene silencing promotes pathology in the mdx mouse model of Duchenne muscular dystrophy. *Hum. Mol. Genet.*, **25**, 2465–2482.
39. Mojumdar, K., Liang, F., Giordano, C., Lemair, C., Danialou, G., Okazaki, T., Bourdon, J., Rafei, M., Galipeau, J., Divangahi, M. and Petrof, B.J. (2014) Inflammatory monocytes promote progression of Duchenne muscular dystrophy and can be therapeutically targeted via CCR2. *EMBO Mol. Med.*, **6**, 1476–1492.
40. Lu, H., Huang, D., Ransohoff, R.M. and Zhou, L. (2011) Acute skeletal muscle injury: CCL2 expression by both monocytes and injured muscle is required for repair. *FASEB J.*, **25**, 3344–3355.
41. Lu, H., Huang, D., Saederup, N., Charo, I.F., Ransohoff, R.M. and Zhou, L. (2010) Macrophages recruited via CCR2 produce insulin-like growth factor-1 to repair acute skeletal muscle injury. *FASEB J.*, **25**, 358–369.
42. Zhao, W., Wang, X., Ransohoff, R.M. and Zhou, L. (2016) CCR2 deficiency does not provide sustained improvement of muscular dystrophy in mdx5cv mice. *FASEB J.*, **31**, 35–46.
43. Warren, G.L., Hulderman, T., Mishra, D., Gao, X., Millecchia, L., O'Farrell, L., Kuziel, W.A. and Simeonova, P.P. (2004) Chemokine receptor CCR2 involvement in skeletal muscle regeneration. *FASEB J.*, **19**, 413–415.
44. Warren, G.L., O'Farrell, L., Summan, M., Hulderman, T., Mishra, D., Luster, M.I., Kuziel, W.A. and Simeonova, P.P. (2004) Role of CC chemokines in skeletal muscle functional restoration after injury. *Am. J. Physiol. Cell Physiol.*, **286**, C1031–C1036.
45. Porter, J.D., Guo, W., Merriam, A.P., Khanna, S., Cheng, G., Zhou, X., Andrade, F.H., Richmonds, C. and Kaminski, H.J. (2003) Persistent over-expression of specific CC class chemokines correlates with macrophage and T-cell recruitment in mdx skeletal muscle. *Neuromuscul. Disord.*, **13**, 223–235.
46. Summan, M., McKinstry, M., Warren, G.L., Hulderman, T., Mishra, D., Brumbaugh, K., Luster, M.I. and Simeonova, P.P. (2003) Inflammatory mediators and skeletal muscle injury: a DNA microarray analysis. *J. Interf. Cytokine Res.*, **23**, 237–245.
47. Kurihara, T., Warr, G., Loy, J. and Bravo, R. (1997) Defects in macrophage recruitment and host defense in mice lacking the CCR2 chemokine receptor. *J. Exp. Med.*, **186**, 1757–1762.
48. Amano, H., Morimoto, K., Senba, M., Wang, H., Ishida, Y., Kumatori, A., Yoshimine, H., Oishi, K., Mukaida, N. and Nagatake, T. (2004) Essential contribution of monocyte chemoattractant protein-1/C-C chemokine ligand-2 to resolution and repair processes in acute bacterial pneumonia. *J. Immunol.*, **172**, 398–409.
49. Rollins, B.J. (1996) Monocyte chemoattractant protein 1: a potential regulator of monocyte recruitment in inflammatory disease. *Mol. Med. Today*, **2**, 198–204.
50. Tidball, J.G. and Wehling-Henricks, M. (2007) Macrophages promote muscle membrane repair and muscle fibre growth and regeneration during modified muscle loading in mice in vivo. *J. Physiol.*, **578**, 327–336.
51. Nguyen, H.X. and Tidball, J.G. (2003) Interactions between neutrophils and macrophages promote macrophage killing of rat muscle cells in vitro. *J. Physiol.*, **547**, 125–132.
52. Cornelio, F. and Dones, I. (1984) Muscle fiber degeneration and necrosis in muscular dystrophy and other muscle diseases: Cytochemical and immunocytochemical data. *Ann. Neurol.*, **16**, 694–701.
53. Briguet, A., Courdier-Fruh, I., Foster, M., Meier, T. and Magyar, J.P. (2004) Histological parameters for the quantitative assessment of muscular dystrophy in the mdx-mouse. *Neuromuscul. Disord.*, **14**, 675–682.
54. Coulton, G.R., Morgan, J.E., Partridge, T.A. and Sloper, J.C. (1988) The mdx mouse skeletal muscle myopathy: I. A histological, morphometric and biochemical investigation. *Neuropathol. Appl. Neurobiol.*, **14**, 53–70.
55. Cai, B., Spencer, M.J., Nakamura, G., Tseng-Ong, L. and Tidball, J.G. (2000) Eosinophilia of dystrophin-deficient muscle is promoted by perforin-mediated cytotoxicity by T cell effectors. *Am. J. Pathol.*, **156**, 1789–1796.
56. Wehling, M., Spencer, M.J. and Tidball, J.G. (2001) A nitric oxide synthase transgene ameliorates muscular dystrophy in mdx mice. *J. Cell Biol.*, **155**, 123–132.
57. Hodgetts, S., Radley, H., Davies, M. and Grounds, M.D. (2006) Reduced necrosis of dystrophic muscle by depletion of host

neutrophils, or blocking TNFα function with Etanercept in mdx mice. *Neuromuscul. Disord.*, **16**, 591–602.
58. Capote, J., Kramerova, I., Martinez, L., Vetrone, S., Barton, E.R., Sweeney, H.L., Miceli, M.C. and Spencer, M.J. (2016) Osteopontin ablation ameliorates muscular dystrophy by shifting macrophages to a pro-regenerative phenotype. *J. Cell Biol.*, **213**, 275–288.
59. Sugiura, S., Lahav, R., Han, J., Kou, S.-Y., Banner, L.R., Pablo, F.D. and Patterson, P.H. (2000) Leukaemia inhibitory factor is required for normal inflammatory responses to injury in the peripheral and central nervous systems in vivo and is chemotactic for macrophages in vitro. *Eur. J. Neurosci.*, **12**, 457–466.
60. Tofaris, G.K., Patterson, P.H., Jessen, K.R. and Mirsky, R. (2002) Denervated Schwann cells attract macrophages by secretion of leukemia inhibitory factor (LIF) and monocyte chemoattractant protein-1 in a process regulated by interleukin-6 and LIF. *J. Neurosci.*, **22**, 6696–6703.
61. Shireman, P.K., Contreras-Shannon, V., Ochoa, O., Karia, B.P., Michalek, J.E. and McManus, L.M. (2007) MCP-1 deficiency causes altered inflammation with impaired skeletal muscle regeneration. *J. Leukoc. Biol.*, **81**, 775–785.
62. Martinez, C.O., McHale, M.J., Wells, J.T., Ochoa, O., Michalek, J.E., McManus, L.M. and Shireman, P.K. (2010) Regulation of skeletal muscle regeneration by CCR2-activating chemokines is directly related to macrophage recruitment. *Am. J. Physiol. Regul. Integr. Comp. Physiol.*, **299**, R832–R842.
63. Brigitte, M., Schilte, C., Plonquet, A., Baba-Amer, Y., Henri, A., Charlier, C., Tajbakhsh, S., Albert, M., Gherardi, R.K. and Chrétien, F. (2010) Muscle resident macrophages control the immune cell reaction in a mouse model of notexin-induced myoinjury. *Arthritis Rheum.*, **62**, 268–279.
64. Henriques-Pons, A., Yu, Q., Rayavarapu, S., Cohen, T.V., Ampong, B., Cha, H.J., Jahnke, V., Van der Meulen, J., Wang, D., Jiang, W. *et al.* (2014) Role of toll-like receptors in the pathogenesis of dystrophin-deficient skeletal and heart muscle. *Hum. Mol. Genet.*, **23**, 2604–2617.
65. Wang, Y., Wehling-Henricks, M., Samengo, G. and Tidball, J.G. (2015) Increases of M2a macrophages and fibrosis in aging muscle are influenced by bone marrow aging and negatively regulated by muscle-derived nitric oxide. *Aging Cell*, **14**, 678–688.
66. Pascual-García, M., Bonfill-Teixidor, E., Planas-Rigol, E., Rubio-Perez, C., Lurlaro, R., Arias, A., Cuartas, I., Sala-Hojman, A., Escudero, L., Martinez-Ricarte, F. *et al.* (2019) LIF regulates CXCL9 in tumor-associated macrophages and prevents CD8+ T cell tumor-infiltration impairing anti-PD1 therapy. *Nat. Commun.*, **10**, 2416.
67. Hunt, L.C., Tudor, E.M. and White, J.D. (2010) Leukemia inhibitory factor-dependent increase in myoblast cell number is associated with phosphotidylinositol 3-kinase-mediated inhibition of apoptosis and not mitosis. *Exp. Cell Res.*, **316**, 1002–1009.
68. Blau, H.M., Webster, C. and Pavlath, G.K. (1983) Defective myoblasts identified in Duchenne muscular dystrophy. *Proc. Natl. Acad. Sci. U. S. A.*, **80**, 4856–4860.
69. Webster, C. and Blau, H.M. (1990) Accelerated age-related decline in replicative life-span of Duchenne muscular dystrophy myoblasts: implications for cell and gene therapy. Somat. *Cell Mol. Genet.*, **16**, 557–565.
70. Sacco, A., Mourkioti, F., Tran, R., Choi, J., Llewellyn, M., Kraft, P., Shkreli, M., Delp, S., Pomerantz, J.H., Artandi, S.E. and Blau, H.M. (2010) Short telomeres and stem cell exhaustion model Duchenne muscular dystrophy in mdx/mTR mice. *Cell*, **143**, 1059–1071.
71. Lu, A., Poddar, M., Tang, Y., Proto, J.D., Sohn, J., Mu, X., Oyster, N., Wang, B. and Huard, J. (2014) Rapid depletion of muscle progenitor cells in dystrophic mdx/utrophin−/− mice. *Hum. Mol. Genet.*, **23**, 4786–4800.
72. Gregorevic, P., Hayes, A., Lynch, G.S. and Williams, D.A. (2000) Functional properties of regenerating skeletal muscle following LIF administration. *Muscle Nerve*, **23**, 1586–1588.
73. Sandow, A. and Brust, M. (1958) Contractility of dystrophic mouse muscle. *Am. J. Physiol.*, **194**, 557–563.
74. Hete, B. and Shung, K.K. (1995) A study of the relationship between mechanical and ultrasonic properties of dystrophic and normal skeletal muscle. *Ultrasound Med. Biol.*, **21**, 343–352.
75. Virgilio, K.M., Martin, K.S., Peirce, S.M. and Blemker, S.S. (2015) Multiscale models of skeletal muscle reveal the complex effects of muscular dystrophy on tissue mechanics and damage susceptibility. *Interface Focus*, **5**, 20140080.
76. White, J.P., Baltgalvis, K.A., Sato, S., Wilson, L.B. and Carson, J.A. (2009) Effect of nandrolone decanoate administration on recovery from bupivacaine-induced muscle injury. *J. Appl. Physiol.*, **107**, 1420–1430.
77. Wehling-Henricks, M., Welc, S.S., Samengo, G., Rinaldi, C., Lindsey, C., Wang, Y., Lee, J., Kuro-O, M. and Tidball, J.G. (2018) Macrophages escape Klotho gene silencing in the mdx mouse model of Duchenne muscular dystrophy and promote muscle growth and increase satellite cell numbers through a Klotho-mediated pathway. *Hum. Mol. Genet.*, **27**, 14–29.
78. Bustin, S.A., Benes, V., Garson, J.A., Hellemans, J., Huggett, J., Kubista, M., Mueller, R., Nolan, T., Pfaffl, M.W., Shipley, G.L., Vandesompele, J. and Wittwer, C.T. (2009) The MIQE guidelines: minimum information for publication of quantitative real-time PCR experiments. *Clin. Chem.*, **55**, 611–622.
79. Nolan, T., Hands, R.E. and Bustin, S.A. (2006) Quantification of mRNA using real-time RT-PCR. *Nat. Protoc.*, **1**, 1559–1582.
80. Vandesompele, J., De Preter, K., Pattyn, F., Poppe, B., Van Roy, N., De Paepe, A. and Speleman, F. (2002) Accurate normalization of real-time quantitative RT-PCR data by geometric averaging of multiple internal control genes. *Genome Biol.*, **3**, research0034.1.